

# Effective theory of light Dirac neutrino portal dark matter with observable $\Delta N_{\text{eff}}$

Debasish Borah<sup>a,b</sup>, Satyabrata Mahapatra<sup>c</sup>, Dibyendu Nanda<sup>d</sup>, Sujit Kumar Sahoo<sup>e</sup>, Narendra Sahu<sup>e</sup>

<sup>a</sup>Department of Physics, Indian Institute of Technology Guwahati, Assam 781039, India

<sup>b</sup>Pittsburgh Particle Physics, Astrophysics, and Cosmology Center, Department of Physics and Astronomy, University of Pittsburgh, Pittsburgh, PA 15260, USA

<sup>c</sup>Department of Physics and Institute of Basic Science, Sungkyunkwan University, Suwon 16419, Korea

<sup>d</sup>Department of Physics, Osaka University, Toyonaka, Osaka 560-0043, Japan

<sup>e</sup>Department of Physics, Indian Institute of Technology Hyderabad, Kandi, Telangana-502285, India.

E-mail: [dborah@iitg.ac.in](mailto:dborah@iitg.ac.in), [satyabrata@g.skku.edu](mailto:satyabrata@g.skku.edu),  
[dnanda@het.phys.sci.osaka-u.ac.jp](mailto:dnanda@het.phys.sci.osaka-u.ac.jp), [ph21resch11008@iith.ac.in](mailto:ph21resch11008@iith.ac.in),  
[nsahu@phy.iith.ac.in](mailto:nsahu@phy.iith.ac.in)

**Abstract.** We study the possibility of light Dirac neutrino portal dark matter (DM) in an effective field theory (EFT) setup. Dirac nature of light neutrino automatically includes its right chiral part  $\nu_R$  which, in our setup, also acts like a portal between DM and the standard model (SM) particles. Considering a Dirac fermion singlet DM stabilised by an unbroken  $Z_2$  symmetry, we write down all possible dimension-6 effective operators involving DM- $\nu_R$  as well as  $\nu_R$ -SM which conserve  $Z_2$ , global lepton number and SM gauge symmetries. DM thermalisation also ensures the thermalisation of  $\nu_R$ , leading to enhanced effective relativistic degrees of freedom  $N_{\text{eff}}$ , within reach of future cosmic microwave background (CMB) experiments. We study the complementarity among DM and CMB related observations for different Lorentz structures of effective operators. We also propose two UV completions based on the popularly studied gauges B – L and left-right symmetric model frameworks.

---

## Contents

<b>1</b>	<b>Introduction</b>	<b>1</b>
<b>2</b>	<b>Effective field theory approach to <math>\Delta N_{\text{eff}}</math> and dark matter</b>	<b>2</b>
2.1	EFT approach to $\Delta N_{\text{eff}}$	3
2.2	Phenomenology of $\nu_R$ -philic dark matter	7
<b>3</b>	<b>UV completion: two examples</b>	<b>13</b>
3.0.1	Doublet Left-Right Model	13
3.0.2	$U(1)_{B-L}$	16
3.1	DM- $\nu_R$ interactions	17
<b>4</b>	<b>Conclusions</b>	<b>17</b>
<b>A</b>	<b>Possible <math>\nu_R</math> interactions with SM bath and their collision terms</b>	<b>18</b>
<b>B</b>	<b>Loop contribution in Direct Detection</b>	<b>18</b>

---

## 1 Introduction

The nature of dark matter (DM) and the origin of neutrino masses remain two of the most pressing questions in particle physics and cosmology [1]. The existence of dark matter is strongly supported by cosmic microwave background (CMB) data and numerous astrophysical observations, including galaxy rotation curves, weak gravitational lensing, and the large-scale structure of the Universe. Recent data from the PLANCK satellite mission [2] indicates that DM constitutes about 26.8% of the total energy density of the Universe. However, none of the standard model (SM) particles meets all the necessary criteria to be a viable DM candidate, leading to the development of numerous beyond the Standard Model (BSM) frameworks.

Similarly, neutrino oscillation experiments [3–7] have revealed that neutrinos possess tiny masses and exhibit large leptonic mixing, which can not be accounted for in the SM where neutrinos remain massless. While these experiments have provided crucial insights regarding the mixing angles and mass squared differences, they remain insensitive to the fundamental nature of neutrinos - whether they are Dirac or Majorana fermions. Although the experiments searching for neutrinoless double-beta decay could potentially confirm the Majorana nature of neutrinos, no such observations have been made to date [1]. This has sparked growing interest in exploring the possibility that light neutrinos could be Dirac fermions, challenging the long-held focus on Majorana neutrinos in conventional neutrino mass models [8–28].

In light of these open questions, there is growing interest in models that connect dark matter and neutrino physics, potentially providing a unified solution to these fundamental puzzles [29–33]. One such approach involves the concept of neutrino portal dark matter, where either SM light neutrinos or heavy neutrinos serve as a mediator between the dark sector and the visible sector [34–46]. Due to the absence of tree level DM-nucleon scattering, this framework is particularly intriguing in light of the null results from direct DM searches. Direct search experiments such as PandaX-II [47], XENON-nT [48, 49], and LUX-ZEPLIN [50] have probed spin-independent DM-nucleon cross-sections down to  $10^{-48}$  GeV<sup>-2</sup> for DM masses

ranging from a few GeV to  $\mathcal{O}(10^4)$  GeV with weaker constraints for lighter DM masses from experiments like DarkSide [51], CDMSlite [52], and CRESST-III [53]. Similar bounds also exist for DM-electron scattering [54]. These null detections motivate the exploration of novel scenarios like neutrino portal DM and their search strategies.

Motivated by these, here we consider right chiral neutrinos ( $\nu_R$ ) introduced to explain light Dirac neutrino mass act like a portal between DM and the visible sector. In earlier works [33, 55, 56], light Dirac neutrino portal DM was studied by considering specific models. In the present work, we adopt a more general effective field theory (EFT) approach, focusing on dimension-6 operators that respect relevant symmetries like the SM gauge symmetries, accidental global symmetries like lepton and baryon numbers and a  $Z_2$  symmetry protecting the stability of DM, chosen to be a vector-like singlet fermion  $\chi$ . The effective interactions of such  $\nu_R$ -philic DM with  $\nu_R$  and interactions of  $\nu_R$  with SM arise at the order of dimension-6 or above. We consider such dimension-6 operators of all possible Lorentz structures. There exist no DM-SM operators at dimension-6 in the spirit of  $\nu_R$ -philic DM, keeping direct detection rates suppressed, in agreement with experimental results.

A key aspect of this scenario is the potential impact on cosmological observables, particularly the effective number of relativistic species ( $N_{\text{eff}}$ ). The thermalisation of right-handed neutrinos in the early Universe can lead to an enhancement in  $N_{\text{eff}}$ , potentially detectable by future CMB experiments. This connection between particle physics and cosmology offers a unique opportunity to probe the dark sector and neutrino properties simultaneously. Our study aims to explore the complementarity between dark matter phenomenology and CMB observations, considering various Lorentz structures of the effective operators. We also propose two ultraviolet (UV) completions based on popular gauge extensions of the SM: the B – L model and the left-right symmetric model. These UV completions provide concrete realizations of the EFT framework and offer additional avenues for experimental tests.

In the following sections, we present our EFT setup, analyze the resulting phenomenology, and discuss implications for future experiments and theoretical model-building in the context of neutrino portal dark matter. Section 2.1 discusses the temperature evolution of  $\nu_R$  and its contribution to  $\Delta N_{\text{eff}}$ , followed by an analysis of DM relic abundance and loop-suppressed direct detection signatures in Section 2.2. Section 3 examines the parameter space of two UV-complete models considering  $\Delta N_{\text{eff}}$  bounds and finally we conclude in Section 4.

## 2 Effective field theory approach to $\Delta N_{\text{eff}}$ and dark matter

The EFT approach serves as a powerful tool to study interactions involving new particles without committing to a specific ultraviolet (UV) completion. By parametrizing the effects of heavy mediators through higher-dimensional operators, EFT provides a model-independent framework that captures a wide range of phenomenological possibilities. This is particularly useful for scenarios where the new physics scale is significantly higher than the energies accessible in current experiments or where direct detection is not feasible. The dark matter phenomenology in such an EFT setup can be discussed with very few free parameters, namely, DM mass, cutoff scale, and the corresponding coupling or Wilson coefficients. Such DM EFT has been studied extensively in the context of direct detection, indirect detection as well as collider searches in several works [57–61], also summarised in a recent review [62].

In this study, we extend the SM particle content by introducing three copies of right-handed neutrinos ( $\nu_R$ ) constituting Dirac neutrinos with  $\nu_L$  in SM and a massive vector-like fermion ( $\chi$ ) that is a candidate for DM with mass  $M_{\text{DM}}(\equiv M_\chi)$ . Both  $\nu_R$  and  $\chi$  are singlets

under the SM gauge group. The vector-like fermion  $\chi$  is stabilised by an additional unbroken  $Z_2$  symmetry, under which all SM particles, including  $\nu_R$  are even. In this framework,  $\nu_R$  carries a leptonic charge similar to SM leptons, keeping light neutrinos purely Dirac in the limit of unbroken global lepton number symmetry. We consider a sub-class of leptophilic DM EFT with light Dirac neutrinos [63] where DM is only ‘ $\nu_R$ -philic’ *i.e.*  $\chi$  interacts exclusively with  $\nu_R$  via EFT operators, making  $\nu_R$  a portal between the visible sector and the dark sector. While this keeps direct detection cross-section of DM highly suppressed at one-loop, it opens up other detection aspects as we discuss in the upcoming sections.

In a minimal setup, we propose the following EFT Lagrangian:

$$\begin{aligned}
-\mathcal{L} \supset & G_S \overline{f_L} \nu_R \overline{\nu_R} f_L + G_V \overline{f_L} \gamma^\mu f_L \overline{\nu_R} \gamma_\mu \nu_R + G_T (\overline{L} \sigma^{\mu\nu} \nu_R \tilde{H} B_{\mu\nu} + \overline{L} \sigma^{\mu\nu} \nu_R \tilde{H} \sigma_i W_{\mu\nu}^i) \\
& + G'_V \overline{\chi_x} \gamma^\mu \chi_x \overline{\nu_R} \gamma_\mu \nu_R + G'_S \overline{\chi_L} \nu_R \overline{\nu_R} \chi_L
\end{aligned} \tag{2.1}$$

where  $x \in L, R$  and  $G_S, G_V, G_T, G'_S, G'_V$  are the dimensionful effective coefficients of the dimension-6 operators. The first three terms describe  $\nu_R$ -SM interactions that can give rise to number changing and elastic scattering processes of  $\nu_R$  with SM fermions  $f_{L,R}$  and lepton doublet,  $L$ , whereas the last two terms represent the interaction between DM and  $\nu_R$ . Since DM interacts only with  $\nu_R$  at leading order while  $\nu_R$  interacts with both SM and DM at the same order, it justifies the  $\nu_R$ -philic nature of DM. Furthermore, the tensor type  $\nu_R$ -SM effective interaction, with coefficient  $G_T$ , can give rise to neutrino magnetic moment (NMM). The measured upper bound on the NMM ( $\mu_\nu$ ) from electron scattering experiment is approximately  $\mu_\nu \sim 2.9 \times 10^{-11} \mu_B$  [64], where  $\mu_B = \frac{e}{2m_e}$  is the Bohr magneton. More recent data from laboratory experiments such as XENONnT [65] and Borexino [66] have provided a significantly stricter limit on the NMM, yielding  $\mu_\nu \sim 6.4 \times 10^{-12} \mu_B$  and  $\mu_\nu \sim 28 \times 10^{-12} \mu_B$ , respectively. In contrast, the astrophysical bound derived from the red giant branch [67], place a much stronger constraint,  $\mu_\nu \sim 1.5 \times 10^{-12} \mu_B$ .

## 2.1 EFT approach to $\Delta N_{\text{eff}}$

The thermalisation of  $\nu_R$  contributes to the effective relativistic degrees of freedom defined as

$$N_{\text{eff}} \equiv \frac{8}{7} \left( \frac{11}{4} \right)^{4/3} \left( \frac{\rho_{\text{Tot}} - \rho_\gamma}{\rho_\gamma} \right), \tag{2.2}$$

where  $\rho_{\text{Tot}}$  is the total radiation content of the Universe with  $\rho_\gamma$  being the photon energy density. CMB measurements constrain such additional relativistic degrees of freedom as  $N_{\text{eff}} = 2.99_{-0.33}^{+0.34}$  at  $2\sigma$  or 95% CL including baryon acoustic oscillation (BAO) data [2]. The translated bound on  $\Delta N_{\text{eff}}$  at  $2\sigma$  can be written as  $\Delta N_{\text{eff}} \lesssim 0.285$ . The latest DESI 2024 data give a slightly weaker bound  $\Delta N_{\text{eff}} \lesssim 0.4$  at  $2\sigma$  CL [68]. Similar bound also exists from big bang nucleosynthesis (BBN)  $2.3 < N_{\text{eff}} < 3.4$  at 95% CL [69]. Both of these cosmological bounds are consistent with the SM predictions  $N_{\text{eff}}^{\text{SM}} = 3.045$  [70–72]. Future CMB experiment CMB-S4 is expected to reach a much better sensitivity of  $\Delta N_{\text{eff}} = N_{\text{eff}} - N_{\text{eff}}^{\text{SM}} = 0.06$  [73], taking it closer to the SM prediction. Another future experiment CMB-HD [74] can probe  $\Delta N_{\text{eff}}$  upto 0.014 at  $2\sigma$ .

There have been several recent works on enhanced  $N_{\text{eff}}$  with Dirac neutrinos [31, 33, 55, 75–93]. EFT of light Dirac neutrino interactions has also been studied in the context of  $N_{\text{eff}}$  [78, 81]. In another recent work [63], EFT of leptophilic DM with light Dirac neutrinos was studied in the context of collider and  $N_{\text{eff}}$  phenomenology. In another recent work [94],

EFT of Dirac neutrino phenomenology was studied upto dimension-6. Here, we consider a similar EFT setup where DM is  $\nu_R$ -philic uniting thermalisation of DM and  $\nu_R$  with the visible sector.

To study the evolution of  $\nu_R$  energy density, we consider the continuity equation for a homogeneous and isotropic Universe:

$$\dot{\rho}_{\text{Tot}} + 3\mathcal{H}(\rho_{\text{Tot}} + P_{\text{Tot}}) = 0, \quad (2.3)$$

where  $\mathcal{H} = \sqrt{\frac{8\pi}{3M_{Pl}^2}\rho_{\text{Tot}}}$  is the Hubble parameter, and  $\rho_{\text{Tot}}$  and  $P_{\text{Tot}}$  are the total energy density and pressure, respectively. These can be decomposed into contributions from the SM bath and  $\nu_R - \chi$  bath as

$$\rho_{\text{Tot}} = \rho_{\text{SM}} + (\rho_{\nu_R} + \rho_{\chi}), \quad (2.4)$$

$$P_{\text{Tot}} = P_{\text{SM}} + (P_{\nu_R} + P_{\chi}). \quad (2.5)$$

The evolution of two separate sectors namely,  $\nu_R$ -DM and the SM bath is described by a coupled system as  $\nu_R$  couples to the SM via similar dimension-6 operators. The effective coupling for  $\chi - \nu_R$  interaction is chosen to be larger than  $0.1 \times G_F$ , ensuring that the DM remained in thermal equilibrium with the  $\nu_R$  bath in the early Universe. While these baths can maintain thermal equilibrium with each other, observational constraints from PLANCK 2018 indicate that for three  $\nu_R$  species, they must have decoupled from the SM plasma at temperatures above 600 MeV [75] - much earlier than the decoupling of left-handed neutrinos ( $\nu_L$ ). When the  $\nu_R$ -SM interaction rate drops below the Hubble rate, the two baths decouple and evolve independently according to

$$\dot{\rho}_{\nu_R} + 3\mathcal{H}(\rho_{\nu_R} + P_{\nu_R}) + 3\mathcal{H}(\rho_{\chi} + P_{\chi}) = C_{\nu_R}^{(\rho)}, \quad (2.6)$$

$$\dot{\rho}_{\text{SM}} + 3\mathcal{H}(\rho_{\text{SM}} + P_{\text{SM}}) = -C_{\nu_R}^{(\rho)}. \quad (2.7)$$

Here,  $C_{\nu_R}^{(\rho)}$  represents the collision term that quantifies energy transfer between the baths through annihilation and scattering processes. For a generic process  $1 + 2 \leftrightarrow 3 + 4$ , this term is given by

$$C_{\nu_R}^{(\rho)} = - N_{\nu_R} \int E_1 d\Pi_1 d\Pi_2 d\Pi_3 d\Pi_4 (2\pi)^4 \delta^4(p_1 + p_2 - p_3 - p_4) \\ \times S \left[ |\mathcal{M}|_{1+2 \rightarrow 3+4}^2 f_1 f_2 (1 - f_3)(1 - f_4) - |\mathcal{M}|_{3+4 \rightarrow 1+2}^2 f_3 f_4 (1 - f_1)(1 - f_2) \right], \quad (2.8)$$

where

$$d\Pi_i = \frac{g_i}{(2\pi)^3} \frac{d^3 p_i}{2E_i}, \quad f_i = \frac{1}{e^{E_i/T_i} + 1}, \quad (i = 1, 2, 3, 4). \quad (2.9)$$

In these equations,  $N_{\nu_R}$  represents the degrees of freedom for  $\nu_R$  species, and  $S$  is the symmetry factor for the relevant processes. Each particle  $i$  is characterized by its internal degrees of freedom ( $g_i$ ), energy ( $E_i$ ), and temperature ( $T_i$ ). Here, it is worth mentioning that, for temperatures around and above the  $\nu_R$ -SM decoupling temperature ( $\gtrsim 500$  MeV), the collision term is dominated by interactions with light SM fermions (electrons and neutrinos), whose masses can be safely neglected at these energy scales.

The evolution equations namely, Eq. (2.6) and Eq. (2.7) can be reformulated to show the temperature evolution of  $\nu_R$  relative to the SM bath temperature as

$$\frac{d\rho_{\nu_R}}{d\rho_{SM}} = \frac{3\mathcal{H}(\rho_{\nu_R} + P_{\nu_R}) + 3\mathcal{H}(\rho_\chi + P_\chi) - C_{\nu_R}^{(\rho)}}{3\mathcal{H}(\rho_{SM} + P_{SM}) - C_{\nu_R}^{(\rho)}}, \quad (2.10)$$

$$\frac{dT_{\nu_R}}{dT_\gamma} = \frac{3\mathcal{H}(\rho_{\nu_R} + P_{\nu_R}) + 3\mathcal{H}(\rho_\chi + P_\chi) - C_{\nu_R}^{(\rho)}}{3\mathcal{H}(\rho_{SM} + P_{SM}) - C_{\nu_R}^{(\rho)}} \frac{\partial\rho_{SM}}{\partial T_\gamma} \left( \frac{\partial\rho_{\nu_R}}{\partial T_{\nu_R}} + \frac{\partial\rho_\chi}{\partial T_{\nu_R}} \right)^{-1}. \quad (2.11)$$

We have calculated the evolution of right-handed neutrino temperature ( $T_{\nu_R}$ ) in the early Universe, focusing on the period when the SM bath temperature ( $T_\gamma$ ) cooled from  $10^6$  MeV down to 10 MeV. The expressions for  $C_{\nu_R}^{(\rho)}$  corresponding to the  $\nu_R$ -SM interactions are provided in Appendix A. We assume the right-handed neutrinos to be thermally equilibrated with the SM bath particles initially. Fig. 1 shows the temperature ratio  $(T_{\nu_R}/T_\gamma)^4$  versus  $T_\gamma$  for different choices of the effective four-fermion interaction strength as mentioned in the inset of the same figure. We show the temperature evolution only for vector-like  $\nu_R$ -SM coupling  $G_V$  and denote its strength relative to the Fermi coupling  $G_F$ . Two benchmark values of DM mass are considered: 0.1 GeV (*left panel*) and 10 GeV (*right panel*). Deviations from the  $(T_{\nu_R}/T_\gamma)^4 = 1$  at lower temperatures indicate the decoupling of  $\nu_R$  bath from the SM bath. The plot shows that a smaller value of  $G_V$  leads to an early decoupling of  $\nu_R$  bath, as expected. In addition to the effective coefficients, the  $T_{\nu_R}$  evolution also depends on DM mass. As noted previously, the DM interacts solely with the  $\nu_R$  bath. Therefore, when  $T_{\nu_R}$  falls below the DM mass, the DM transfers its entropy to the  $\nu_R$  thermal bath. At this epoch, if the  $\nu_R$  bath remains in equilibrium with the SM thermal bath, the ratio  $T_{\nu_R}/T_\gamma$  will remain constant due to quick dissipation of  $\nu_R$  energy into the SM bath. However, if the  $\nu_R$  thermal bath has decoupled from the SM thermal bath, the entropy discharge from the DM leads to an increase in  $\nu_R$  bath temperature. This behaviour is clearly shown in Fig. 1. In the *left panel*, the  $\nu_R$  bath is completely decoupled from the SM bath at  $T_\gamma \simeq 10^3$  MeV for all the showcased  $G_V$  values. In this scenario, DM of mass 0.1 GeV slows down the fall in  $T_{\nu_R}$  across all coloured contours for  $T_{\nu_R} \lesssim 10^2$  MeV. In the *right panel*, DM of mass 10 GeV transfers its entropy during the epoch of  $1 \text{ GeV} \lesssim T_\gamma \lesssim 10 \text{ GeV}$ . The purple and orange coloured contours correspond to the decoupling of  $\nu_R$  from the SM bath before  $T_\gamma \simeq 10^4$  MeV, and receive the maximum entropy contribution from the DM, leading to an increase in  $T_{\nu_R}$  once  $T_{\nu_R} \simeq M_{DM}$ . In contrast, the red coloured contour shows  $\nu_R$ -SM decoupling at  $T_{\nu_R} \simeq 1$  GeV and does not receive any further contribution from DM entropy transfer. The green and blue contours show  $\nu_R$ -SM decoupling in the same epoch when DM transfers entropy to  $\nu_R$  bath. Between these two contours, the green contour corresponds to earlier  $\nu_R$ -SM decoupling, leading to a larger  $T_{\nu_R}/T_\gamma$  ratio, as it receives a greater contribution from the DM entropy transfer compared to the blue contour. We also find similar behaviour of  $T_{\nu_R}$  evolution for both scalar and tensor type interactions.

The contribution of  $\nu_R$  to the effective number of neutrino species  $N_{\text{eff}}$  can be expressed as:

$$\Delta N_{\text{eff}} = N_\nu \left( \frac{11}{4} \right)^{4/3} \frac{\rho_{\nu_R,0}}{\rho_{SM,0}} = N_\nu \left( \frac{11}{4} \right)^{4/3} \frac{T_{\nu_R,0}^4}{T_{\gamma,0}^4} \quad (2.12)$$

$$= N_\nu \left( \frac{T_{\nu_R,10}}{T_{\gamma,10}} \right)^4, \quad (2.13)$$

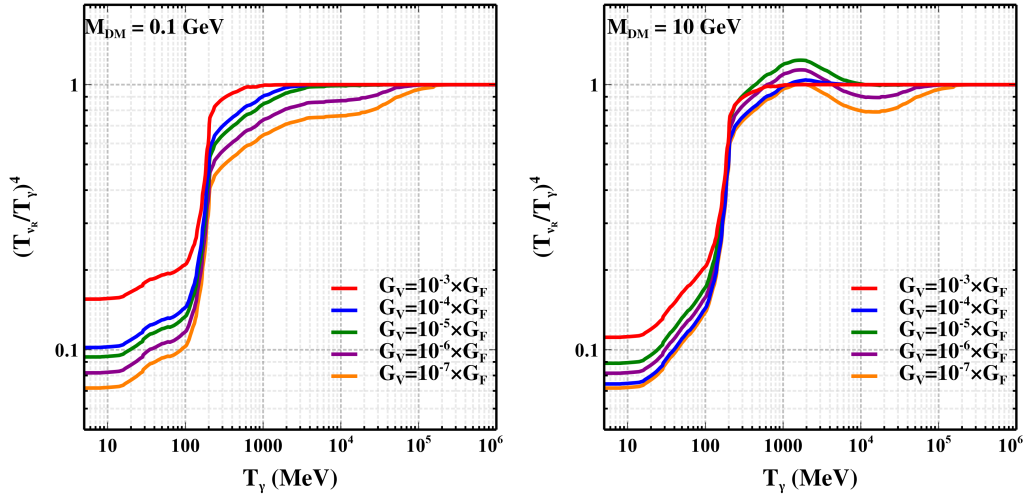


**Figure 1:** The evolution of  $(T_{\nu_R}/T_\gamma)^4$  for several benchmark values of  $G_V$  with  $M_{\text{DM}} = 0.1$  GeV (*left*) and 10 GeV (*right*).

where subscript “0” refers to the CMB formation temperature and “10” indicates a photon bath temperature of 10 MeV.

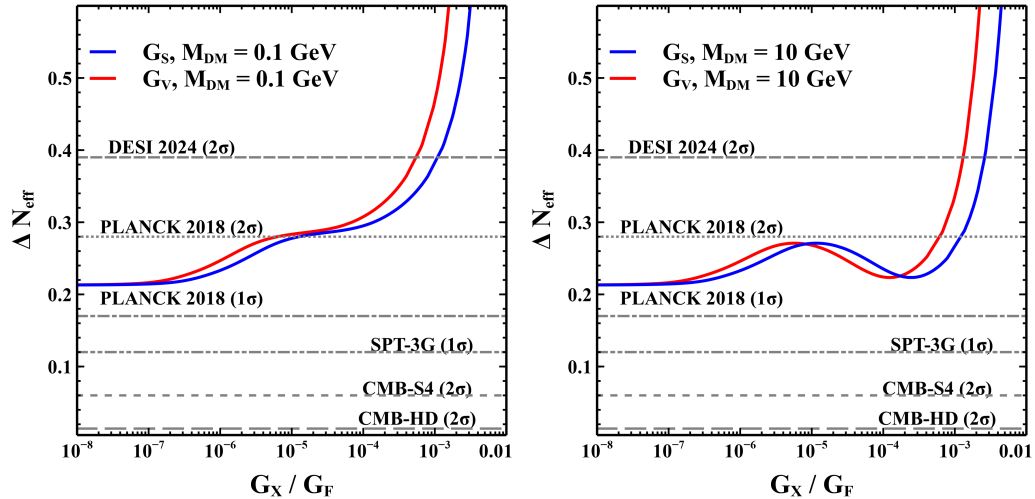


**Figure 2:**  $\Delta N_{\text{eff}}$  as a function of  $G_X$  ( $X \equiv S, V$ ) with  $M_{\text{DM}} = 0.1$  GeV (*left*) and 10 GeV (*right*). We have shown the current upper bounds from PLANCK 2018 [2] and the analysis by [95] using the recent DESI 2024 data. The sensitivity of upcoming experiments SPT-3G [96], CMB-S4 [73] and CMB-HD [74] are also shown.

In Fig. 2, we showcase the  $\Delta N_{\text{eff}}$  due to  $\nu_R$  as a function of the effective couplings  $G_S$  and  $G_V$ , for  $M_{\text{DM}} = 0.1$  GeV (*left*) and 10 GeV (*right*). In the horizontal axis, the strength of  $G_S$  and  $G_V$  are shown relative to the Fermi constant  $G_F$ . In both *left* and *right* panel plots, for  $G_X < 10^{-5} \times G_F$ ,  $\nu_R$  decouples before  $T_\gamma \simeq 10$  GeV, resulting in an equal contribution to  $\Delta N_{\text{eff}}$  for both the DM masses with a minimum value  $\Delta N_{\text{eff}} \approx 0.21$ . It should be noted that the minimum value of  $\Delta N_{\text{eff}}$  may vary depending on the DM mass, in general. In the *left*



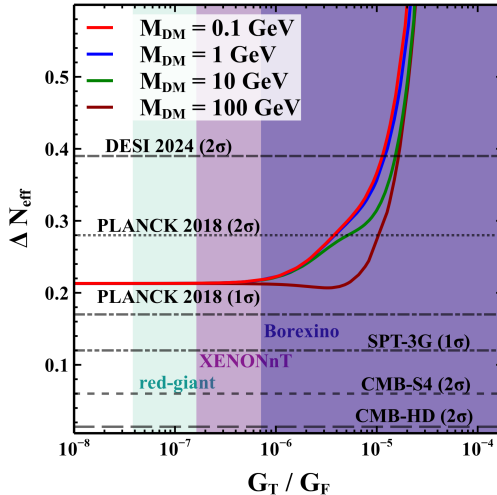


**Figure 3:**  $\Delta N_{\text{eff}}$  as a function of  $G_T$  is shown for  $M_{\text{DM}} = (0.1, 1, 10, 100)$  GeV. The shaded regions represent the values of  $G_T$  that are excluded by the NMM constraints. The current upper bounds and future sensitivities from CMB experiments are indicated by the horizontal grey lines.

panel, the behaviour of the contour can be easily understood as the increase in  $G_X$  leads to a late decoupling from the SM bath followed by a rise in  $T_{\nu_R}$  from the DM entropy transfer resulting in a monotonic increase in  $\Delta N_{\text{eff}}$ . In the *right* panel, a dip is observed around  $G_X \simeq 10^{-4} \times G_F$ , which results from the interplay between the epochs of the  $\nu_R$  decoupling and entropy transfer from DM. We have shown the existing constraints from PLANCK 2018 and recent results of DESI 2024. We also project the future sensitivities of SPT-3G, CMB-S4 and CMB-HD. While PLANCK 2018 results rule out  $G_S/G_F$  and  $G_V/G_F$  larger than  $5.7 \times 10^{-6}$ , DESI 2024 results allows  $G_S$  and  $G_V$  as large as  $5.6 \times 10^{-4}$ . Notably, the projected sensitivities of future experiments like SPT-3G, CMB-S4 and CMB-HD can completely probe these scenarios in which  $\nu_R$  is thermalised with SM bath in the early Universe. Similarly, Fig. 3 illustrates the contribution to  $\Delta N_{\text{eff}}$  arising from the  $\nu_R$ -SM tensorial interaction term as a function of the respective coupling  $G_T$ . The variation in  $\Delta N_{\text{eff}}$  for  $M_{\text{DM}} = (0.1, 1, 10, 100)$  GeV is shown as coloured contours. The horizontal grey lines represent the current bounds and future sensitivities from CMB experiments, while the shaded regions indicate the exclusion limit due to upper bound on Dirac NMM from experiments such as XENONnT [65], Borexino [66] and astrophysical observations related to red-giants [67]. We have used these limits to constrain the effective tensorial operator,  $G_T$ , and it excludes  $G_T \geq 3.82 \times 10^{-8} G_F$ . Due to the presence of DM interacting via  $\nu_R$ -portal, we get enhanced contribution to  $N_{\text{eff}}$  compared to a scenario without DM [97].

## 2.2 Phenomenology of $\nu_R$ -philic dark matter

### DM Relic Density:

In this section, we explore the relic density of vector-like fermionic dark matter ( $\chi$ ), which interacts exclusively with right-handed neutrinos ( $\nu_R$ ) through dimension-6 effective operators. These interactions are crucial in determining the annihilation of DM into  $\nu_R$  as shown in Fig. 4 and the resulting relic density. The relevant terms in the EFT Lagrangian include: a scalar-type interaction, governed by the effective coupling  $G'_S$  (*i.e.*  $G'_S \bar{\chi} L \nu_R \bar{\nu}_R \chi L$ ) and a



vector-type interaction proportional to effective coupling  $G'_V$  (i.e.  $G'_V \bar{\chi}_x \gamma^\mu \chi_x \bar{\nu}_R \gamma_\mu \nu_R$  where  $x \equiv L, R$ ). In a UV complete framework, the scalar interaction can contribute to a  $t$ -channel annihilation process of the DM, whereas the vector interaction can contribute to a  $s$ -channel annihilation of DM into  $\nu_R$ .

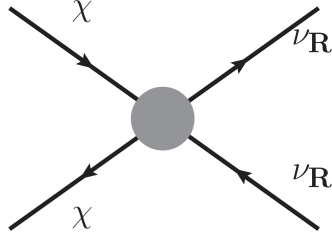


**Figure 4:** DM annihilation to  $\nu_R$ .

In subsection 2.1, we discussed the evolution of the  $\nu_R$  thermal bath temperature relative to the SM temperature, as illustrated in Fig. 1. As DM  $\chi$  exclusively interacts with  $\nu_R$ , the thermal evolution of  $\nu_R$  bath directly impacts the dynamics of DM freeze-out. Notably, it can give rise to two distinct scenarios as follows.

1. Early freeze-out: If dark matter freezes out before  $\nu_R$  decouples from the SM bath, the conventional freeze-out mechanism applies. In this case, the SM bath temperature governs the whole process.
2. Late freeze-out: When dark matter freeze-out occurs after  $\nu_R$  decoupling, a more complex scenario emerges. Here,  $\nu_R$  and dark matter form a separate thermal bath, necessitating appropriate consideration of both SM and  $\nu_R$  bath temperatures in the Boltzmann equations.

The temperature of right-handed neutrinos  $T_{\nu_R}$  is expressed as a function of the SM bath temperature ( $T_\gamma$ ), with their decoupling governed by the effective coefficient  $G_X$ . Initially, when temperatures are high,  $T_{\nu_R}$  closely tracks  $T_\gamma$ . As the Universe cools,  $\nu_R$  eventually decouples from the SM bath, with the epoch of decoupling determined by  $G_X$ . A larger  $G_X$  value delays the decoupling, resulting in a higher  $T_{\nu_R}$  at later epochs relative to scenarios with smaller  $G_X$ . The Boltzmann equation governing the evolution of comoving DM density can then be expressed as [98]

$$\frac{dY_\chi}{dx} = -\beta(T_\gamma) \frac{s(T_\gamma)}{\mathcal{H}(T_\gamma, T_{\nu_R}, M_{\text{DM}})} \frac{1}{x} \langle \sigma v \rangle \left( Y_\chi^2 - (Y_\chi^{\text{eq}})^2 \right), \quad (2.14)$$

where  $x = M_{\text{DM}}/T_\gamma$ ,  $M_{\text{DM}}$  is the mass of  $\chi$  and  $\langle \sigma v \rangle$  is the thermally averaged cross-section of  $\bar{\chi}\chi \rightarrow \bar{\nu}_R\nu_R$ . The other relevant quantities appearing in the above Boltzmann equation

can be defined as

$$Y_\chi = \frac{n_\chi}{s}, \quad n_\chi(T_{\nu_R}, M_{\text{DM}}) = \frac{g_\chi}{2\pi} T_{\nu_R} M_{\text{DM}}^2 K_2 \left( \frac{M_{\text{DM}}}{T_{\nu_R}} \right), \quad (2.15)$$

$$s(T_\gamma) = \frac{2\pi^2}{45} g_{*s}(T_\gamma) T_\gamma^3, \quad (2.16)$$

$$\mathcal{H}(T_\gamma, T_{\nu_R}, M_{\text{DM}}) = \sqrt{\frac{8\pi}{3M_{\text{pl}}^2} \rho_{\text{Tot}}(T_\gamma, T_{\nu_R}, M_{\text{DM}})}, \quad (2.17)$$

$$\beta(T_\gamma) = 1 + \frac{T_\gamma}{3g_{*s}(T_\gamma)} \frac{dg_{*s}(T_\gamma)}{dT_\gamma}, \quad (2.18)$$

$$\sigma(\bar{\chi}\chi \rightarrow \bar{\nu}_R\nu_R) = \frac{G_V'^2}{4\pi} \frac{1}{s} \left( \frac{s^2}{3} + \frac{2M_{\text{DM}}^2 s}{3} - 2M_{\text{DM}}^4 \right) \left( 1 - \frac{4M_{\text{DM}}^2}{s} \right)^{-1/2}. \quad (2.19)$$

Here  $g_\chi$  is the internal degrees of freedom of  $\chi$ ,  $g_{*s}(T_\gamma)$  is the effective degrees of freedom,  $\rho_{\text{Tot}} (= \rho_\gamma(T_\gamma) + \rho_{\nu_R}(T_{\nu_R}) + \rho_\chi(T_{\nu_R}, M_{\text{DM}}))$  is the total energy density, and  $M_{\text{pl}}$  is the Planck mass ( $= 1.22 \times 10^{19}$  GeV).

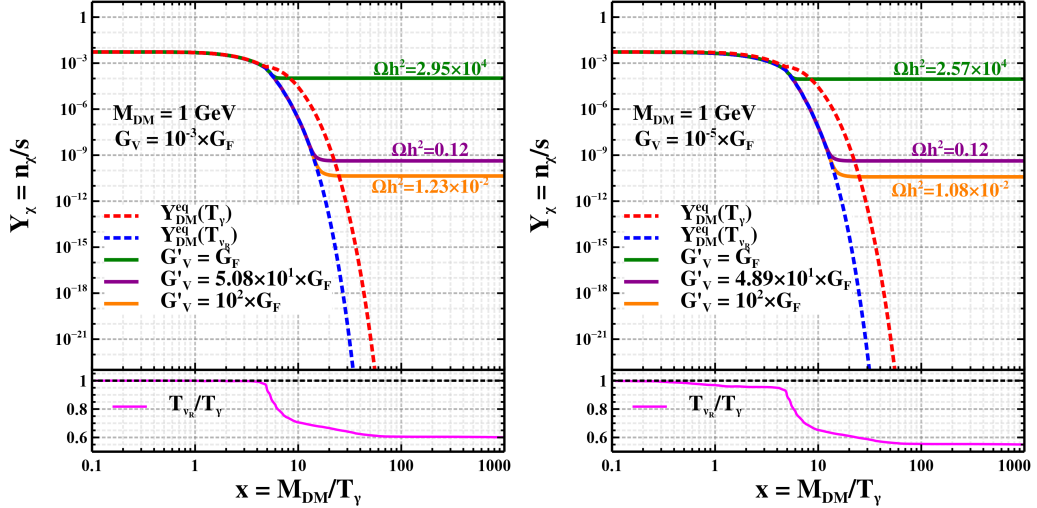


**Figure 5:** Here we have shown the evolution of DM abundance (top) and  $(T_{\nu_R}/T_\gamma)$  (magenta line in the bottom panels) with respect to  $x = M_{\text{DM}}/T_\gamma$ . The bottom panels depict the  $\nu_R$  decoupling from SM thermal bath.

Fig. 5 illustrates the evolution of DM number density, obtained by solving the Boltzmann equation (cf. Eq. (2.14)). We present results for a benchmark DM mass of 1 GeV, considering three different values of the coupling constant  $G'_V$ . As  $G'_V$  increases, the interaction rate rises, leading to delayed DM decoupling and consequently, a reduced DM relic abundance. As discussed previously, the DM dynamics are primarily governed by the temperature of the right-handed neutrino ( $\nu_R$ ) bath, which in turn depends on its interaction rate with the SM bath, controlled by the effective operator coefficient  $G_X$ . The bottom insets of Fig. 5 depict the corresponding evolution of  $T_{\nu_R}$  relative to the photon temperature  $T_\gamma$ . The magenta line ( $T_{\nu_R}/T_\gamma$ ) deviates from the thick black dotted line ( $T_{\nu_R}/T_\gamma = 1$ ), indicating the decoupling of  $\nu_R$  from the SM bath. The blue dashed line represents the equilibrium abundance of

DM as a function of  $T_{\nu_R}$ , while the red dashed line shows the equilibrium DM density as a function of the photon temperature  $T_\gamma$ . Once  $\nu_R$  decouples from the SM bath, these two lines diverge. For a given value of  $x$ , the blue line corresponds to a lower equilibrium abundance compared to the red line, reflecting the impact of the decoupled  $\nu_R$  bath on DM evolution. We investigated two scenarios for the decoupling temperature of  $\nu_R$  by solving the Boltzmann equation for DM evolution. The left plot showcases a late decoupling scenario for  $\nu_R$ , with  $G_X(=G_V) = 10^{-3} \times G_F$ , while the right plot illustrates an earlier decoupling scenario, where  $G_X(=G_V) = 10^{-5} \times G_F$ . In both plots, the green and orange lines correspond to identical  $G'_V$  values as mentioned in the inset of the figure. Notably, the earlier  $\nu_R$  decoupling scenario (right plot) results in a lower relic density compared to the late  $\nu_R$  decoupling scenario (left plot). The purple line in both plots represents the correct relic density, achieved by fine-tuning the  $G'_V$  coefficients. As anticipated, the earlier  $\nu_R$  decoupling scenario requires a smaller  $G'_V$  value to attain the correct relic density, reflecting the need for earlier DM decoupling.

In Fig. 6, we summarise the correct relic density parameter space in the plane of  $\Delta N_{\text{eff}}$  and DM mass (lower x-axis) ranging from 0.1 GeV to 100 GeV, while different colours of solid contours represent the effective coefficient  $G_S$  in the *left panel* and  $G_V$  in the *right panel*. For a fixed value of  $G_S$  (or  $G_V$ ), the DM mass and  $G'_V$  show one-to-one correspondence to provide correct relic density, which is shown in the upper x-axis. For simplicity, we consider only vector-type effective interactions for the DM. We constrain the DM mass to be below the EFT scale. The DM annihilation cross-section increases with the center-of-mass energy and, consequently, with DM mass [99]. As the cross-section grows with increasing mass, a smaller effective coefficient is required to achieve the correct relic density. This inverse relationship is clearly demonstrated in the figure, where lower  $G'_V$  values correspond to larger DM masses. Similarly, in Fig. 7, we present the DM relic density that satisfies the parameter space for three benchmark values of  $G_T$ . As shown in Fig. 3, a substantial range of  $G_T$  values is ruled out by the NMM bounds. However, there exists a narrow range of  $G_T (< 3.82 \times 10^{-8} G_F)$  where the thermal relic density of  $\nu_R$  can contribute minimally to  $\Delta N_{\text{eff}} (\simeq 0.21)$ .

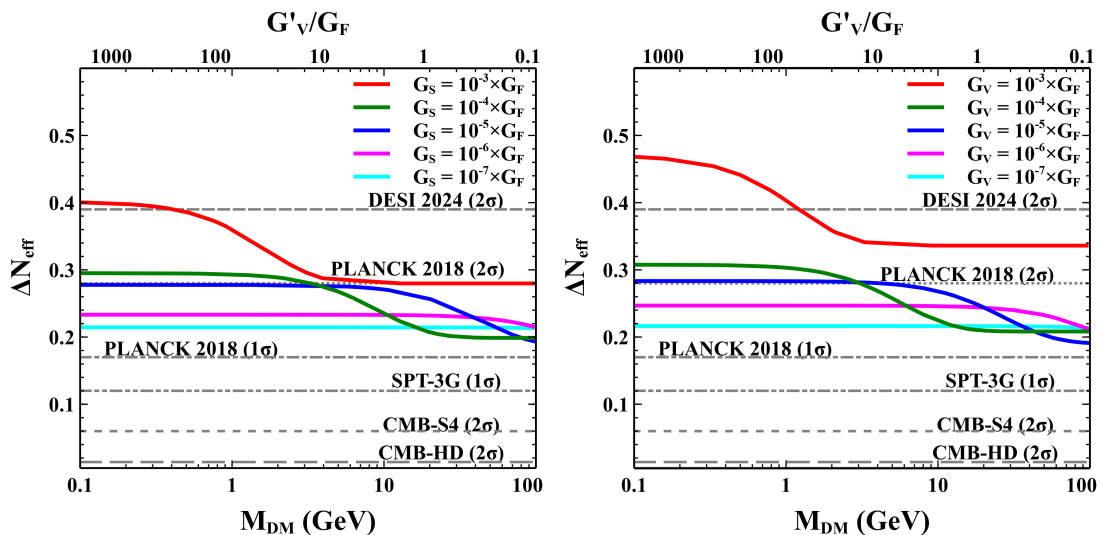


**Figure 6:** Relic satisfying points are plotted in the plane of DM mass and  $\Delta N_{\text{eff}}$ . In the *left panel*, the coloured contours represent the corresponding effective coefficient  $G_S$ , while in the *right panel*, they represent the corresponding  $G_V$  value.

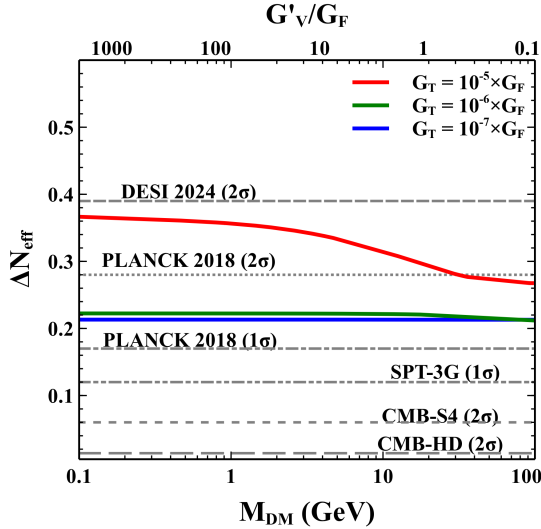


**Figure 7:** Relic satisfying points are plotted in the plane of DM mass and  $\Delta N_{\text{eff}}$ . The coloured contours represent the corresponding  $G_T$  value.

#### Direct Detection:

In the  $\nu_R$ -philic DM model, DM lacks direct interactions with the SM and hence DM-

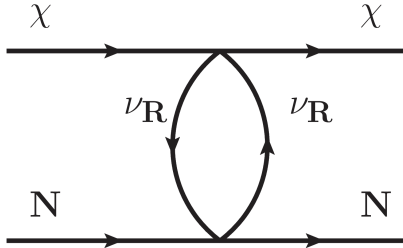


**Figure 8:** DM-nucleon scattering processes for DM direct detection.

nucleon scattering is not possible at the tree-level. However, DM direct detection remains feasible through a loop-mediated process involving right-handed neutrinos ( $\nu_R$ ), as illustrated in Fig. 8. The direct detection cross-section for loop-level DM-nucleon scattering is given by:

$$\sigma_{\chi N} = \int_0^{4v^2\mu_{\chi N}^2} dp^2 \frac{1}{64\pi} \frac{1}{M_{\text{DM}}^2 M_N^2} \frac{1}{v^2} \overline{|\mathcal{M}_{\chi N}|^2}, \quad (2.20)$$

where the reduced mass of the DM-nucleon system is given as,  $\mu_{\chi N} = \frac{M_{\text{DM}} M_N}{M_{\text{DM}} + M_N}$ . We assume a DM velocity of  $v \sim 10^{-3}$  for DM in the galactic halo. The amplitude of the loop diagram  $|\mathcal{M}_{\chi N}|^2$  is detailed in Appendix B. In Fig. 9, we present the spin-independent DM-nucleus scattering cross-section as a function of DM mass (thick coloured lines) along with the existing experimental constraints (dotted lines). The solid lines represent the DM-nucleus scattering cross-section for benchmark values of  $G'_V$  scaled with  $G_F$ , with  $G_V$  fixed at  $10^{-3} \times G_F$ . The dashed lines show the experimental bounds from XENON [48, 49], LUX-ZEPLIN(LZ) [50], CDMSlite [52], CRESST-III [53], DarkSide-50 Binomial Fluctuation [51] and PandaX-II [47]. The grey shaded region shows the neutrino floor [100]. For each  $G'_V$  value, we impose a

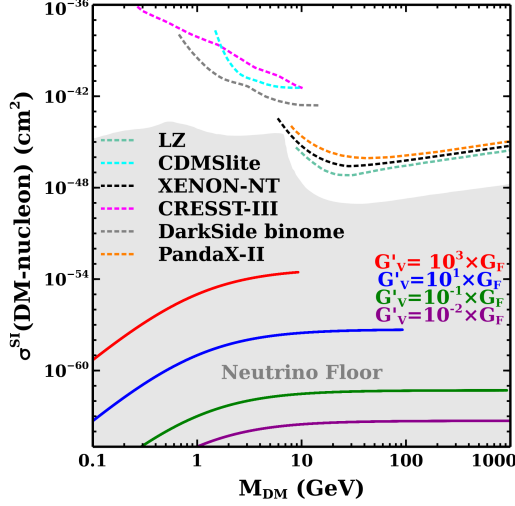


**Figure 9:** Spin-independent DM-nucleon scattering cross-section as a function of DM mass.

perturbative-unitarity cut-off on the DM mass to ensure the validity of the EFT treatment. This can be seen from some of the solid contours appearing only below a certain value of DM mass. The loop contribution significantly suppresses the direct detection cross-section, placing it far below the present and future sensitivity of DM direct search experiments. Consequently, this  $\nu_R$ -philic DM scenario could potentially explain the null detection of DM in terrestrial direct detection facilities.

#### Indirect Detection:

In addition to direct detection, our  $\nu_R$ -philic DM model allows for indirect detection through loop-induced processes involving  $\nu_R$ . These processes enable DM annihilation to charged fermions, which can be constrained by various gamma-ray and cosmic-ray experiments as well as from CMB anisotropy.

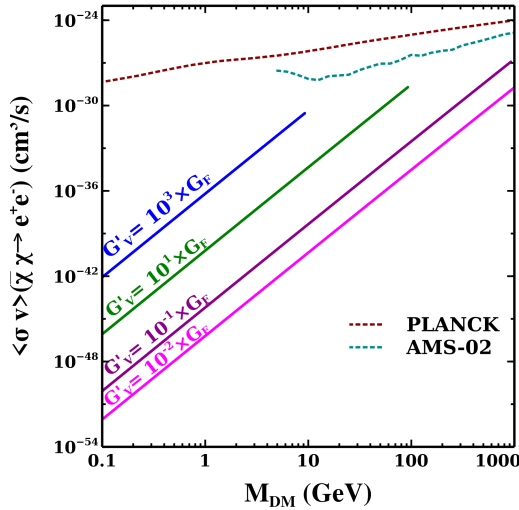


**Figure 10:** DM annihilation cross-section  $\langle \sigma v \rangle_{\bar{\chi}\chi \rightarrow e^+e^-}$  as a function of DM mass

Fig. 10 illustrates the thermal averaged annihilation cross-section of DM to  $e^+e^-$  via the

$s$ -wave channel as a function of DM mass. We present results for several benchmark values of  $G'_V$  scaled with  $G_F$ . The solid lines represent the annihilation cross-section, while the dashed lines show the current observational bounds from CMB measurement [101] and AMS02 [102]. Similar to the case of direct detection, here also we apply the upper bound on DM mass from validity of EFT, as seen for the chosen values of effective couplings in green and blue coloured contours.

### 3 UV completion: two examples

In this section, we briefly discuss two possible UV completions where light Dirac neutrino and  $\nu_R$ -philic DM can arise naturally. They are based on the popular BSM frameworks based on left-right symmetry and gauged  $U(1)_{B-L}$  symmetry.

#### 3.0.1 Doublet Left-Right Model

The left-right symmetric model (LRSM) is one of the most popular BSM frameworks, and different versions of LRSM have been studied in the literature [14, 103–113]. Here, the SM gauge symmetry is extended to  $SU(3)_c \times SU(2)_L \times SU(2)_R \times U(1)_{B-L}$ , where right-handed fermions, singlets in the SM, form doublets under  $SU(2)_R$ . This naturally incorporates right-handed neutrinos ( $\nu_R$ ) and treats left- and right-handed fermions equally. Here, we adopt the very first proposals of LRSM where a scalar bidoublet ( $\Phi$ ) had been considered for generating the masses of quarks  $Q_{L,R}$  and leptons  $l_{L,R}$  as well as electroweak symmetry breaking, and two scalar doublets ( $\zeta_L$  and  $\zeta_R$ ) for left-right symmetry breaking at high scales [103–107]. In this minimal Doublet Left-Right Model (DLRM), all fermions, including neutrinos, acquire Dirac masses via Yukawa coupling with the bidoublet scalar. Achieving sub-eV neutrino masses in this framework requires Yukawa couplings  $< 10^{-12}$ . However, due to the gauge interactions, the right-handed neutrinos can have different phenomenological consequences.

The relevant Yukawa Lagrangian for the mass generation of the fermions is given by,

$$-\mathcal{L} \supset h_{ij} \bar{l}_{L,i} \Phi l_{R,j} + \tilde{h}_{ij} \bar{l}_{L,i} \tilde{\Phi} l_{R,j} + g_{ij} \bar{Q}_{L,i} \Phi Q_{R,j} + \tilde{g}_{ij} \bar{Q}_{L,i} \tilde{\Phi} Q_{R,j} + \text{h.c.}, \quad (3.1)$$

where the indices  $i, j$  represent the 3 generations of lepton and quark,  $\tilde{\Phi} = \sigma_2 \phi^* \sigma_2$  and  $\sigma_2$  is the Pauli matrix. The VEVs of the neutral component of the scalar fields are given by,

$$\langle \Phi \rangle = \begin{pmatrix} \frac{k_1}{\sqrt{2}} & 0 \\ 0 & \frac{k_2}{\sqrt{2}} \end{pmatrix}, \quad \langle \zeta_L \rangle = \begin{pmatrix} 0 \\ \frac{v_L}{2} \end{pmatrix}, \quad \langle \zeta_R \rangle = \begin{pmatrix} 0 \\ \frac{v_R}{2} \end{pmatrix}, \quad (3.2)$$

where the VEVs  $k_1, k_2$  satisfy the VEV of SM,  $v_{SM} = \sqrt{k_1^2 + k_2^2} \approx 246$  GeV. The spontaneous symmetry breaking of the DLRM to  $U(1)_{EM}$  results in two charged massive vector bosons ( $W_L^\pm, W_R^\pm$ ), two neutral massive vector bosons ( $Z_L, Z_R$ ) and one neutral massless photon ( $A$ ) [114]. The charge fermion and neutrino mass can be written as

$$M_l = \frac{1}{\sqrt{2}}(hk_2 + \tilde{h}k_1), \quad M_\nu = \frac{1}{\sqrt{2}}(hk_1 + \tilde{h}k_2), \quad (3.3)$$

where we have suppressed the generation index of the leptons. As mentioned above, such Yukawa couplings involved in the neutrino mass generation are extremely small and can not provide any phenomenological effects in present cosmological or terrestrial experiments. However, due to the presence of the gauge interactions, the RHNs can interact and exchange

energy with the SM plasma and the relevant annihilation and scattering processes are shown in Fig. 11. The collision terms for these processes are given by

$$C^{(\rho)}(\nu_R \bar{\nu}_R \leftrightarrow \ell_R \bar{\ell}_R (f \bar{f})) = 0.8841 \times \frac{8}{\pi^5} |G_1 - G_2|^2 (T_\gamma^9 - T_{\nu_R}^9) \quad (3.4)$$

$$C^{(\rho)}(\nu_R \bar{\ell}_R \leftrightarrow \nu_R \bar{\nu}_R) = 0.8518 \times \frac{2}{\pi^5} |G_1 - G_2|^2 T_\gamma^4 T_{\nu_R}^4 (T_\gamma - T_{\nu_R}), \quad (3.5)$$

where  $G_1$  and  $G_2$  are the effective coefficients of the  $W_R^+$  and  $Z_R$  mediated interactions, respectively and can be expressed as,

$$G_1 = \frac{g_R^2}{2M_{W_R}^2}, G_2 = \frac{g_R^2 + 2g_{BL}^2}{4M_{Z_R}^2}, \quad (3.6)$$

where the mixing angles between  $W_R$  and  $W_L$ , and  $Z_R$  and  $Z_L$  are assumed to be less than  $\mathcal{O}(0.1)$ . One important point about the DLRM is that the gauge couplings ( $g_R, U(1)_{B-L}$ ) corresponding to  $SU(2)_R$  and  $U(1)_{B-L}$  gauge symmetry can not be arbitrarily chosen rather they have to obey the following relation

$$\frac{1}{g_Y^2} = \frac{1}{g_R^2} + \frac{1}{g_{BL}^2}. \quad (3.7)$$

due to the symmetry breaking pattern  $SU(2)_R \times U(1)_{B-L} \rightarrow U(1)_Y$ . As the  $g_Y$  is already known, one can vary the  $g_R$  and  $g_{BL}$  within the allowed range subjected to the perturbative limits. The blue contour line in Fig. 12 shows the allowed value of  $g_R$  and  $g_{BL}$ , where the shaded regions are restricted from the perturbative limits on  $g_R$  and  $g_{BL}$ . Such couplings can thermalise RHNs in the early Universe through their inaction with  $W_R$  and  $Z_R$ . In Fig. 13

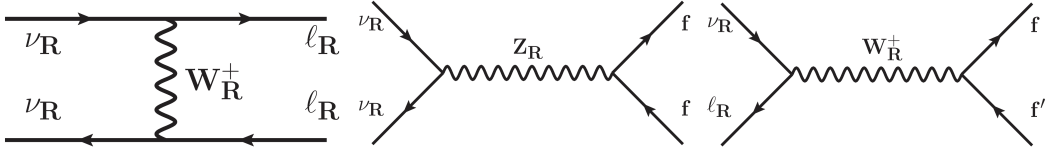


**Figure 11:** Processes involved in energy exchange between  $\nu_R$  bath and SM bath.

(left), we have shown the  $\Delta N_{\text{eff}}$  contribution from  $\nu_R$  where the plot shows the dependency of  $\Delta N_{\text{eff}}$  on the effective coefficient. The contribution to  $\Delta N_{\text{eff}}$  increases with a larger effective coefficient, which depends on the fermion-gauge boson coupling and the gauge boson mass mediating the interaction. Notably, there is a minimum contribution of 0.14 to  $\Delta N_{\text{eff}}$ , even for small coefficients. The right plot shows the parameter space of coupling ( $g_R$ ) and gauge boson mass ( $M_{W_R}$ ), highlighting the region allowed by CMB constraints. The blue and red arcs on the left correspond to DESI 2024 [68, 95] and PLANCK 2018 [2] bounds, respectively.

The mean lifetime of the muon is precisely measured to be  $(2.1969811 \pm 0.0000022) \times 10^{-6}$  s [1]. In this model, the right chiral current introduces new decay channels, as shown in Fig. 14, where the constraint from the muon lifetime is more stringent than that from the tau lifetime. The partial decay width of muon for the decay channel shown in Fig. 14 can be found as

$$\Gamma(\ell_R^i \rightarrow \ell_R^j \nu_R^i \bar{\nu}_R^j) = \frac{G_V^2 M_{\ell^i}^5}{192\pi^3}. \quad (3.8)$$

One can constrain the DLRM parameter space, from the criteria of keeping this partial decay width within limits. The excluded region is shown as the magenta shaded area in Fig. 13.



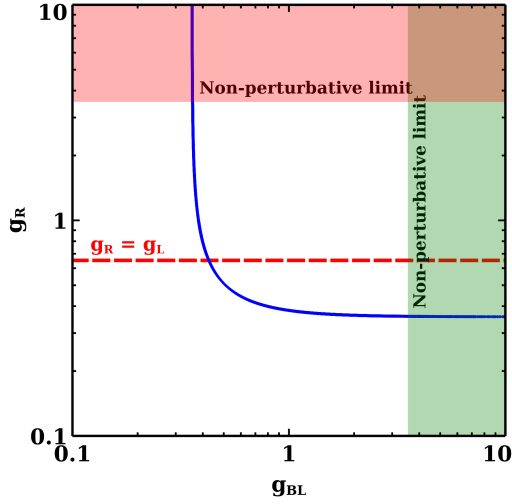


**Figure 12:** Allowed parameter space in the plane of  $g_R$  and  $g_{BL}$ , where the red dashed line corresponds to  $g_R = g_L = 0.652$ .

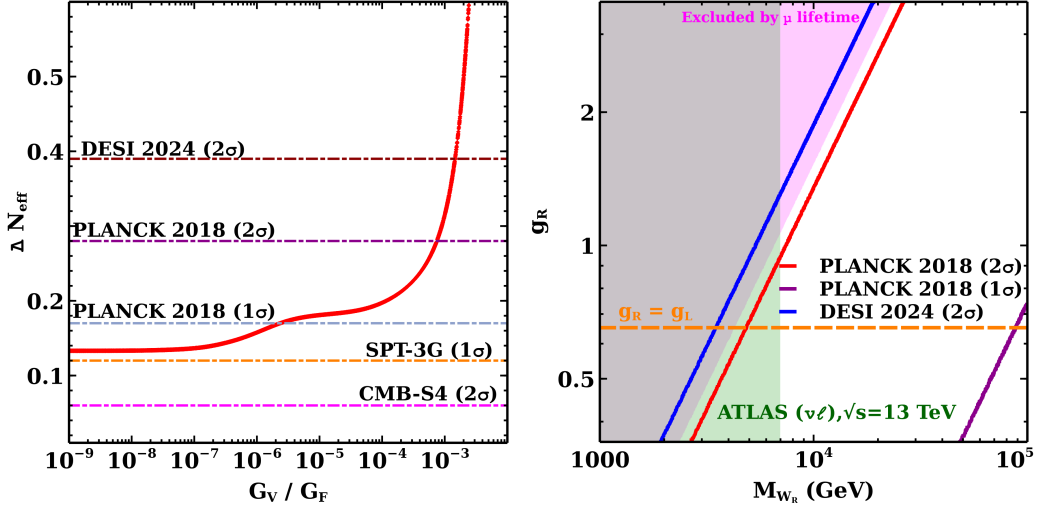


**Figure 13:** (Left) The contribution of  $\nu_R$  to  $\Delta N_{\text{eff}}$ . (Right) The allowed parameter space is shown in the plane of  $g_R$  and  $M_{W_R}$ , where the mixing between  $W_R$  and  $W_L$  is approximated to be  $10^{-3}$ . The green shaded region depicts the bound from ATLAS [115].

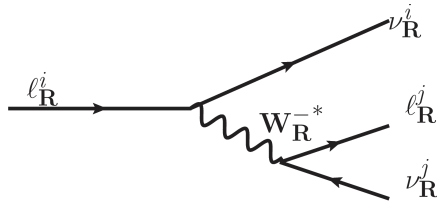


**Figure 14:** New contribution to the leptonic decay in the DLRM model.

### 3.0.2 $U(1)_{B-L}$

Gauged  $B - L$  extension of the SM [109, 116–120] has been another BSM framework studied extensively in the literature. Here also, the inclusion of three right handed neutrinos becomes a natural requirement for anomaly cancellation. In order to prevent Majorana mass of right handed neutrinos, one can have an unbroken  $U(1)_{B-L}$  with a massive neutral gauge boson,  $Z'$ , using the Stueckelberg mechanism [76]. Alternatively, one can choose the scalar content in a way which breaks  $B - L$  symmetry by more than 2 units to forbid the Majorana mass term [121]. The Dirac mass term can be generated from the usual Yukawa Lagrangian, given by

$$\mathcal{L} \supset y_{\alpha\beta} \bar{l}_{L\alpha} \tilde{H} \nu_{R\beta} + \text{h.c.}, \quad (3.9)$$

where  $\alpha$  and  $\beta$  are flavour indices,  $l_L$  is the lepton doublet,  $\tilde{H} = i\sigma_2 H^*$ . The Yukawa couplings ( $y_{\alpha\beta}$ ) are required to be sufficiently small to generate the observed small neutrino masses, consistent with the neutrino mass scale inferred from experimental data. In addition to the Yukawa interactions, the RHNs couple to SM fermions through gauge interactions, with the exchange of a  $Z'$  boson. Analogous to the DLRM framework discussed above, we computed the collision terms for the interactions between  $\nu_{RS}$  and SM fermions and, subsequently, their contribution to the  $\Delta N_{\text{eff}}$ . In Fig. 15, we present the allowed parameter space in  $M_{Z'} - g_{BL}$  plane based on the constraints coming from DESI 2024 [68, 95] and PLANCK 2018 [2], indicated by the coloured solid lines. The shaded regions correspond to the updated constraints coming from various other experiments, such as CMS [122], ATLAS [123], LHCb [124], BABAR [125], COHERENT [126], BOREXINO [127], Beam-dump [128], E137 [129], Supernova-Colling [130], on the gauge coupling ( $g_{BL}$ ) for the  $Z'$  boson mass, within the range of  $10^{-2}$  GeV to  $10^5$  GeV.

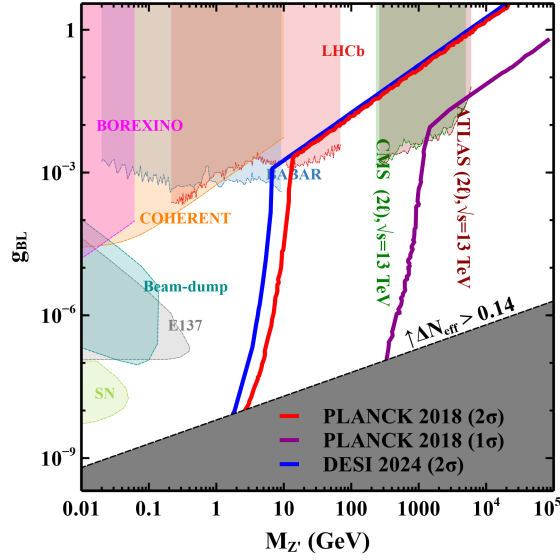


**Figure 15:** The allowed parameter space is presented in the  $g_{BL}$  vs  $M_{Z'}$  plane. The blue line represents the constraint on  $\Delta N_{\text{eff}}$  from the DESI 2024 results at the  $2\sigma$  CL. Similarly, the red and purple lines correspond to the  $2\sigma$  and  $1\sigma$  constraints on  $\Delta N_{\text{eff}}$  from the PLANCK 2018 data, respectively. The grey shaded region represents the out of equilibrium condition for  $\nu_R/Z'$ .

### 3.1 DM- $\nu_R$ interactions

The two examples of UV completions discussed above, right handed neutrinos are included automatically ensuring  $\nu_R$  thermalisation with the SM bath. However, dark matter has to be included separately in such a way that DM- $\nu_R$  effective operators can be realised at low energy. Assuming DM to be singlet Dirac fermion  $\chi$  with zero  $B-L$  charge, we can incorporate DM- $\nu_R$  interaction by introducing another scalar field. An unbroken  $Z_2$  symmetry under which  $\chi$  is odd while all other fields are even can stabilise DM. In DLRM, since  $\nu_R$  is part of  $SU(2)_R$  doublet, an inert scalar doublet  $\eta_R$  can be introduced which allows Yukawa type interaction  $\bar{l}_R \tilde{\eta}_R \chi$ . The inert scalar doublet  $\eta_R$  is also odd under  $Z_2$  and heavier than DM, as required to ensure the stability of the latter. Similarly, in the  $U(1)_{B-L}$  model, we need to introduce a  $Z_2$ -odd singlet scalar  $\zeta$  with  $B-L$  charge 1 such that Yukawa interaction of the type  $\bar{\chi} \zeta \nu_R$  can be realised. Such Yukawa type interactions, after integrating out the heavy inert scalars, lead to effective operators of scalar type  $G'_{S\bar{X}L\nu_R\nu_R\bar{X}L}$  discussed earlier. Similar UV completions can be worked out to realise other Lorentz structures of the effective operators as well.

## 4 Conclusions

In this work, we have studied an effective field theory of light Dirac neutrinos and dark matter, assuming the latter to interact with the standard model only via right chiral parts of Dirac neutrinos. Assuming DM to be a vector-like singlet fermion stabilised by an unbroken  $Z_2$  symmetry, we systematically write down effective operators of the lowest possible dimension involving DM- $\nu_R$  and  $\nu_R$ -SM interactions. This naturally connects the thermalisation of DM with that of  $\nu_R$  leading to enhancement of the effective relativistic degrees of freedom  $N_{\text{eff}}$ , within reach of future CMB experiments. We found that the relic abundance of dark matter is intricately tied to the temperature evolution of the  $\nu_R$  bath, which is further influenced by its interactions with the SM bath. This allows one to distinguish two distinct freeze-out scenarios, each with unique implications for the dark matter parameter space. We also find enhancement of  $N_{\text{eff}}$  in the presence of both DM- $\nu_R$  and  $\nu_R$ -SM interactions compared to the scenarios without DM discussed in earlier works. While typical direct and indirect detection prospects of such DM remain suppressed in agreement with null results, future CMB experiments bring complementary detection avenues.

Finally, we studied two ultraviolet completions of the EFT operators discussed in the beginning: the doublet Left-Right Symmetric Model and the  $U(1)_{B-L}$  gauge extension with light Dirac neutrinos. These models naturally incorporate right-handed neutrinos thereby accommodating light Dirac neutrinos and offer interesting complementarity between detection prospects at CMB and collider experiments. Inclusion of DM in such setups can further enhance  $\Delta N_{\text{eff}}$  improving the detection prospects.

## Acknowledgments

The work of D.B. is supported by the Science and Engineering Research Board (SERB), Government of India grants MTR/2022/000575 and CRG/2022/000603. D.B. also acknowledges the support from the Fulbright-Nehru Academic and Professional Excellence Award 2024-25. S.M. acknowledges the financial support from National Research Foundation (NRF) grant funded by the Korea government (MEST) Grant No. NRF-2022R1A2C1005050. The work of D.N. is partially supported by JSPS Grant-in-Aid for JSPS Research Fellows No. 24KF0238. S.K.S. would like to thank Xun-Jie Xu for valuable discussions and insights.

## A Possible $\nu_R$ interactions with SM bath and their collision terms

Following the four-fermion effective terms in Eq. (2.1), the energy transfer between the  $\nu_R$  and SM baths happen through the interactions,

$$\nu_R + \bar{\nu}_R \leftrightarrow f_L + \bar{f}_L, \quad (\text{A.1})$$

$$\nu_R + f_L \leftrightarrow \nu_R + \bar{f}_L, \quad (\text{A.2})$$

$$\nu_R + \bar{f}_L \leftrightarrow \nu_R + f_L, \quad (\text{A.3})$$

$$\nu_R + \bar{\nu}_L \leftrightarrow \bar{f} + f. \quad (\text{A.4})$$

The collision terms for the scalar and vector type interactions are given in Table 1, and for tensorial interactions, we have followed the prescription given in [94].

process	$C_{\nu_R}^{(\rho)}$ from MB statistics	$1 - \delta_{\text{FD}}$
$\nu_R(p_1) + \bar{\nu}_R(p_2) \leftrightarrow \nu_L(p_3) + \bar{\nu}_L(p_4)$	$\frac{2}{\pi^5}  G_S - 2G_V ^2 N_{\nu_R} (T_{\text{SM}}^9 - T_{\nu_R}^9)$	0.8841
$\nu_R(p_1) + \nu_L(p_2) \leftrightarrow \nu_R(p_3) + \nu_L(p_4)$	$\frac{1}{2\pi^5}  G_S - 2G_V ^2 N_{\nu_R} T_{\text{SM}}^4 T_{\nu_R}^4 (T_{\text{SM}} - T_{\nu_R})$	0.8518
$\nu_R(p_1) + \bar{\nu}_L(p_2) \leftrightarrow \nu_R(p_3) + \bar{\nu}_L(p_4)$	$\frac{3}{\pi^5}  G_S - 2G_V ^2 N_{\nu_R} T_{\text{SM}}^4 T_{\nu_R}^4 (T_{\text{SM}} - T_{\nu_R})$	0.8249

**Table 1:** Collision terms  $C_{\nu_R}^{(\rho)}$

## B Loop contribution in Direct Detection

The loop factor, for the diagram given in Fig. 8, is given by

$$I = \frac{G_V G'_V}{(2\pi)^4} \int d^4 k \frac{\not{k}}{k^2 + i\epsilon} \frac{\not{p} + \not{k}}{(p+k)^2 + i\epsilon}. \quad (\text{B.1})$$

The integration above diverges for large loop momentum, so we employ dimensional regularization to regularize the integration. In  $n$ -dimension, the integration takes the form

$$I = \frac{G_V G'_V \mu^{4-n}}{(2\pi)^n} \int d^n k \frac{\not{k}}{k^2 + i\epsilon} \frac{\not{p} + \not{k}}{(p+k)^2 + i\epsilon} \quad (\text{B.2})$$

$$= \frac{n G_V G'_V \mu^{4-n}}{(2\pi)^n} \int d^n k \frac{p \cdot k + k^2}{(k^2 + i\epsilon)((p+k)^2 + i\epsilon)}, \quad (\text{B.3})$$

where  $k$  is the loop momentum,  $p$  is the momentum transfer from  $\chi$  to nucleus and  $\mu$  is chosen to have mass dimension 1. Using the Feynman parameter,  $x$ , and replacing  $k \rightarrow k - px$ , one can write the Eq. (B.3) as

$$I = \frac{n G_V G'_V \mu^{4-n}}{(2\pi)^n} \int_0^1 dx \int d^n k \frac{k^2 - \overline{Q^2}}{(k^2 + \overline{Q^2})^2}, \quad (\text{B.4})$$

where  $\overline{Q^2} = x(1-x)p^2$ . After applying Wick's rotation ( $d^n k \rightarrow id^n l_E = idl_E l_E^{n-1} d\Omega_{n-1} = id\Omega_{n-1} \frac{1}{2} dl_E^2 l_E^{n-2}$ ,  $k^2 \rightarrow -l_E^2$  and  $p^2 \rightarrow -p_E^2$ ) and simplifying

$$I = \frac{-in G_V G'_V \mu^{4-n}}{(2\pi)^n} \frac{2\pi^{n/2}}{\Gamma(n/2)} \frac{1}{2} \int_0^1 dx \int_0^\infty dl_E^2 \frac{l_E^{n-2} (l_E^2 - Q^2)}{(l_E^2 + Q^2)^2}, \quad (\text{B.5})$$

where  $Q^2 = x(1-x)p_E^2$  and we used  $\int d\Omega_{n-1} = \frac{2\pi^{n/2}}{\Gamma(n/2)}$ . For further simplification, we used variable replacement  $\frac{l_E^2}{Q^2} \rightarrow \xi$  and the Eq. (B.5) can be read as,

$$I = \frac{-inG_V G'_V \mu^{4-n}}{(2\pi)^n} \frac{\pi^{n/2}}{\Gamma(n/2)} \int_0^1 dx Q^{n-2} \int_0^\infty d\xi \frac{\xi^{\frac{n}{2}-1}(\xi-1)}{(\xi+1)^2} \quad (\text{B.6})$$

$$= iG_V G'_V \left[ \frac{p_E^2}{8\pi^2 \epsilon} + \frac{p_E^2}{8\pi^2} \left( \gamma_E - \frac{3}{2} + \ln \frac{p_E^2}{4\pi\mu^2} \right) + \mathcal{O}(\epsilon) \right], \quad (\text{B.7})$$

where  $\gamma_E$  is defined as Euler's constant and carries a value of 0.577216 and  $n = 4 - 2\epsilon$ . While solving from Eq. (B.6) to Eq. (B.7), we used the definition of  $\beta$ -function,  $\beta(m+1, n+1) = \int_0^\infty \frac{du u^m}{(1+u)^{m+n+2}}$ . We note that the loop factor can be regularized for any finite value of  $\epsilon$ . Now, applying Wick's rotation on Eq. (B.7),

$$I = -iG_V G'_V \left[ \frac{p^2}{8\pi^2} \left( \gamma_E - \frac{3}{2} + \ln \left| \frac{p^2}{4\pi\mu^2} \right| - i\pi \right) + \mathcal{O}(\epsilon) \right] \quad (\text{B.8})$$

Eq. (B.8) represents the effective coefficient of the DM-nucleus scattering through a loop mediated process. For practical purposes, one may choose the  $\mu$  value such that the logarithmic term can be neglected.

$$\overline{|\mathcal{M}_{\chi N}|^2} = 16 (Z\alpha_p + (A-Z)\alpha_n)^2 M_{\text{DM}}^2 M_N^2 |I|^2 \quad (\text{B.9})$$

where  $A, Z$  are mass number and atomic number, respectively,  $\alpha_{p,n} \simeq 3$  and  $M_n$  is the nucleon mass.

## References

- [1] **Particle Data Group** Collaboration, S. Navas *et al.*, *Review of particle physics*, *Phys. Rev. D* **110** (2024), no. 3 030001.
- [2] **Planck** Collaboration, N. Aghanim *et al.*, *Planck 2018 results. VI. Cosmological parameters*, *Astron. Astrophys.* **641** (2020) A6, [[arXiv:1807.06209](#)]. [Erratum: *Astron. Astrophys.* 652, C4 (2021)].
- [3] **Super-Kamiokande** Collaboration, Y. Fukuda *et al.*, *Evidence for oscillation of atmospheric neutrinos*, *Phys. Rev. Lett.* **81** (1998) 1562–1567, [[hep-ex/9807003](#)].
- [4] **SNO** Collaboration, Q. R. Ahmad *et al.*, *Measurement of the rate of  $\nu_e + d \rightarrow p + p + e^-$  interactions produced by  $^8\text{B}$  solar neutrinos at the Sudbury Neutrino Observatory*, *Phys. Rev. Lett.* **87** (2001) 071301, [[nucl-ex/0106015](#)].
- [5] **Double Chooz** Collaboration, Y. Abe *et al.*, *Indication of Reactor  $\bar{\nu}_e$  Disappearance in the Double Chooz Experiment*, *Phys. Rev. Lett.* **108** (2012) 131801, [[arXiv:1112.6353](#)].
- [6] **Daya Bay** Collaboration, F. P. An *et al.*, *Observation of electron-antineutrino disappearance at Daya Bay*, *Phys. Rev. Lett.* **108** (2012) 171803, [[arXiv:1203.1669](#)].
- [7] **RENO** Collaboration, J. K. Ahn *et al.*, *Observation of Reactor Electron Antineutrino Disappearance in the RENO Experiment*, *Phys. Rev. Lett.* **108** (2012) 191802, [[arXiv:1204.0626](#)].
- [8] P. Minkowski,  *$\mu \rightarrow e\gamma$  at a Rate of One Out of  $10^9$  Muon Decays?*, *Phys. Lett. B* **67** (1977) 421–428.

- [9] M. Gell-Mann, P. Ramond, and R. Slansky, *Complex Spinors and Unified Theories*, *Conf. Proc. C* **790927** (1979) 315–321, [[arXiv:1306.4669](#)].
- [10] R. N. Mohapatra and G. Senjanovic, *Neutrino Mass and Spontaneous Parity Nonconservation*, *Phys. Rev. Lett.* **44** (1980) 912.
- [11] O. Sawada and A. Sugamoto, eds., *Proceedings: Workshop on the Unified Theories and the Baryon Number in the Universe: Tsukuba, Japan, February 13-14, 1979*, (Tsukuba, Japan), Natl.Lab.High Energy Phys., 1979.
- [12] T. Yanagida, *Horizontal Symmetry and Masses of Neutrinos*, *Prog. Theor. Phys.* **64** (1980) 1103.
- [13] J. Schechter and J. W. F. Valle, *Neutrino Masses in  $SU(2) \times U(1)$  Theories*, *Phys. Rev. D* **22** (1980) 2227.
- [14] R. N. Mohapatra and G. Senjanovic, *Neutrino Masses and Mixings in Gauge Models with Spontaneous Parity Violation*, *Phys. Rev. D* **23** (1981) 165.
- [15] J. Schechter and J. W. F. Valle, *Neutrino Decay and Spontaneous Violation of Lepton Number*, *Phys. Rev. D* **25** (1982) 774.
- [16] C. Wetterich, *Neutrino Masses and the Scale of  $B-L$  Violation*, *Nucl. Phys. B* **187** (1981) 343–375.
- [17] G. Lazarides, Q. Shafi, and C. Wetterich, *Proton Lifetime and Fermion Masses in an  $SO(10)$  Model*, *Nucl. Phys. B* **181** (1981) 287–300.
- [18] B. Brahmachari and R. N. Mohapatra, *Unified explanation of the solar and atmospheric neutrino puzzles in a minimal supersymmetric  $SO(10)$  model*, *Phys. Rev. D* **58** (1998) 015001, [[hep-ph/9710371](#)].
- [19] R. Foot, H. Lew, X. G. He, and G. C. Joshi, *Seesaw Neutrino Masses Induced by a Triplet of Leptons*, *Z. Phys. C* **44** (1989) 441.
- [20] M. Dutta, S. Bhattacharya, P. Ghosh, and N. Sahu, *Singlet-Doublet Majorana Dark Matter and Neutrino Mass in a minimal Type-I Seesaw Scenario*, *JCAP* **03** (2021) 008, [[arXiv:2009.00885](#)].
- [21] D. Borah, M. Dutta, S. Mahapatra, and N. Sahu, *Singlet-doublet self-interacting dark matter and radiative neutrino mass*, *Phys. Rev. D* **105** (2022), no. 7 075019, [[arXiv:2112.06847](#)].
- [22] D. Borah, S. Mahapatra, and N. Sahu, *Singlet-doublet fermion origin of dark matter, neutrino mass and  $W$ -mass anomaly*, *Phys. Lett. B* **831** (2022) 137196, [[arXiv:2204.09671](#)].
- [23] P. Konar, A. Mukherjee, A. K. Saha, and S. Show, *Linking pseudo-Dirac dark matter to radiative neutrino masses in a singlet-doublet scenario*, *Phys. Rev. D* **102** (2020), no. 1 015024, [[arXiv:2001.11325](#)].
- [24] P. Konar, A. Mukherjee, A. K. Saha, and S. Show, *A dark clue to seesaw and leptogenesis in a pseudo-Dirac singlet doublet scenario with (non)standard cosmology*, *JHEP* **03** (2021) 044, [[arXiv:2007.15608](#)].
- [25] S. Bhattacharya, N. Sahoo, and N. Sahu, *Singlet-Doublet Fermionic Dark Matter, Neutrino Mass and Collider Signatures*, *Phys. Rev. D* **96** (2017), no. 3 035010, [[arXiv:1704.03417](#)].
- [26] S. Bhattacharya, B. Karmakar, N. Sahu, and A. Sil, *Flavor origin of dark matter and its relation with leptonic nonzero  $\theta_{13}$  and Dirac  $CP$  phase  $\delta$* , *JHEP* **05** (2017) 068, [[arXiv:1611.07419](#)].
- [27] D. Borah, S. Mahapatra, P. K. Paul, N. Sahu, and P. Shukla, *Asymmetric self-interacting dark matter with a canonical seesaw model*, *Phys. Rev. D* **110** (2024), no. 3 035033, [[arXiv:2404.14912](#)].

- [28] P. K. Paul, N. Sahu, and P. Shukla, *Thermal leptogenesis, dark matter and gravitational waves from an extended canonical seesaw*, [arXiv:2409.08828](#).
- [29] C.-Y. Yao and G.-J. Ding, *Systematic Study of One-Loop Dirac Neutrino Masses and Viable Dark Matter Candidates*, *Phys. Rev. D* **96** (2017), no. 9 095004, [[arXiv:1707.09786](#)].  
[Erratum: *Phys.Rev.D* 98, 039901 (2018)].
- [30] C. D. R. Carvajal and O. Zapata, *One-loop Dirac neutrino mass and mixed axion-WIMP dark matter*, *Phys. Rev. D* **99** (2019), no. 7 075009, [[arXiv:1812.06364](#)].
- [31] D. Nanda and D. Borah, *Connecting Light Dirac Neutrinos to a Multi-component Dark Matter Scenario in Gauged  $B - L$  Model*, *Eur. Phys. J. C* **80** (2020), no. 6 557, [[arXiv:1911.04703](#)].
- [32] D. Borah, S. Mahapatra, D. Nanda, and N. Sahu, *Inelastic fermion dark matter origin of XENON1T excess with muon  $(g - 2)$  and light neutrino mass*, *Phys. Lett. B* **811** (2020) 135933, [[arXiv:2007.10754](#)].
- [33] N. Das and D. Borah, *Light Dirac neutrino portal dark matter with gauged  $U(1)B-L$  symmetry*, *Phys. Rev. D* **109** (2024), no. 7 075045, [[arXiv:2312.06777](#)].
- [34] A. Falkowski, J. Juknevich, and J. Shelton, *Dark Matter Through the Neutrino Portal*, [arXiv:0908.1790](#).
- [35] V. Gonzalez Macias and J. Wudka, *Effective theories for Dark Matter interactions and the neutrino portal paradigm*, *JHEP* **07** (2015) 161, [[arXiv:1506.03825](#)].
- [36] B. Batell, T. Han, and B. Shams Es Haghi, *Indirect Detection of Neutrino Portal Dark Matter*, *Phys. Rev. D* **97** (2018), no. 9 095020, [[arXiv:1704.08708](#)].
- [37] B. Batell, T. Han, D. McKeen, and B. Shams Es Haghi, *Thermal Dark Matter Through the Dirac Neutrino Portal*, *Phys. Rev. D* **97** (2018), no. 7 075016, [[arXiv:1709.07001](#)].
- [38] P. Bandyopadhyay, E. J. Chun, R. Mandal, and F. S. Queiroz, *Scrutinizing Right-Handed Neutrino Portal Dark Matter With Yukawa Effect*, *Phys. Lett. B* **788** (2019) 530–534, [[arXiv:1807.05122](#)].
- [39] M. Chianese and S. F. King, *The Dark Side of the Littlest Seesaw: freeze-in, the two right-handed neutrino portal and leptogenesis-friendly fimpzillas*, *JCAP* **09** (2018) 027, [[arXiv:1806.10606](#)].
- [40] M. Blennow, E. Fernandez-Martinez, A. Olivares-Del Campo, S. Pascoli, S. Rosauero-Alcaraz, and A. V. Titov, *Neutrino Portals to Dark Matter*, *Eur. Phys. J. C* **79** (2019), no. 7 555, [[arXiv:1903.00006](#)].
- [41] J. M. Lamprea, E. Peinado, S. Smolenski, and J. Wudka, *Self-interacting neutrino portal dark matter*, *Phys. Rev. D* **103** (2021), no. 1 015017, [[arXiv:1906.02340](#)].
- [42] M. Chianese, B. Fu, and S. F. King, *Minimal Seesaw extension for Neutrino Mass and Mixing, Leptogenesis and Dark Matter: FIMPzillas through the Right-Handed Neutrino Portal*, *JCAP* **03** (2020) 030, [[arXiv:1910.12916](#)].
- [43] P. Bandyopadhyay, E. J. Chun, and R. Mandal, *Feeble neutrino portal dark matter at neutrino detectors*, *JCAP* **08** (2020) 019, [[arXiv:2005.13933](#)].
- [44] E. Hall, T. Konstandin, R. McGehee, and H. Murayama, *Asymmetric matter from a dark first-order phase transition*, *Phys. Rev. D* **107** (2023), no. 5 055011, [[arXiv:1911.12342](#)].
- [45] A. Berlin and N. Blinov, *Thermal neutrino portal to sub-MeV dark matter*, *Phys. Rev. D* **99** (2019), no. 9 095030, [[arXiv:1807.04282](#)].
- [46] X.-J. Xu, S. Zhou, and J. Zhu, *The  $\nu_R$ -philic scalar dark matter*, *JCAP* **04** (2024) 012, [[arXiv:2310.16346](#)].
- [47] **PandaX-II** Collaboration, X. Cui *et al.*, *Dark Matter Results From 54-Ton-Day Exposure of PandaX-II Experiment*, *Phys. Rev. Lett.* **119** (2017), no. 18 181302, [[arXiv:1708.06917](#)].



- [48] **XENON** Collaboration, E. Aprile *et al.*, *First Dark Matter Search with Nuclear Recoils from the XENONnT Experiment*, *Phys. Rev. Lett.* **131** (2023), no. 4 041003, [[arXiv:2303.14729](#)].
- [49] **XENON** Collaboration, E. Aprile *et al.*, *Search for Light Dark Matter Interactions Enhanced by the Migdal Effect or Bremsstrahlung in XENON1T*, *Phys. Rev. Lett.* **123** (2019), no. 24 241803, [[arXiv:1907.12771](#)].
- [50] **LZ** Collaboration, J. Aalbers *et al.*, *First Dark Matter Search Results from the LUX-ZEPLIN (LZ) Experiment*, *Phys. Rev. Lett.* **131** (2023), no. 4 041002, [[arXiv:2207.03764](#)].
- [51] **DarkSide** Collaboration, P. Agnes *et al.*, *Low-Mass Dark Matter Search with the DarkSide-50 Experiment*, *Phys. Rev. Lett.* **121** (2018), no. 8 081307, [[arXiv:1802.06994](#)].
- [52] **SuperCDMS** Collaboration, R. Agnese *et al.*, *Search for Low-Mass Dark Matter with CDMSlite Using a Profile Likelihood Fit*, *Phys. Rev. D* **99** (2019), no. 6 062001, [[arXiv:1808.09098](#)].
- [53] **CRESST** Collaboration, A. H. Abdelhameed *et al.*, *First results from the CRESST-III low-mass dark matter program*, *Phys. Rev. D* **100** (2019), no. 10 102002, [[arXiv:1904.00498](#)].
- [54] **XENON** Collaboration, E. Aprile *et al.*, *Light Dark Matter Search with Ionization Signals in XENON1T*, *Phys. Rev. Lett.* **123** (2019), no. 25 251801, [[arXiv:1907.11485](#)].
- [55] A. Biswas, D. Borah, and D. Nanda, *Light Dirac neutrino portal dark matter with observable  $\Delta N_{\text{eff}}$* , *JCAP* **10** (2021) 002, [[arXiv:2103.05648](#)].
- [56] A. Biswas, D. Borah, N. Das, and D. Nanda, *Freeze-in dark matter via a light Dirac neutrino portal*, *Phys. Rev. D* **107** (2023), no. 1 015015, [[arXiv:2205.01144](#)].
- [57] M. Beltran, D. Hooper, E. W. Kolb, and Z. C. Krusberg, *Deducing the nature of dark matter from direct and indirect detection experiments in the absence of collider signatures of new physics*, *Phys. Rev. D* **80** (2009) 043509, [[arXiv:0808.3384](#)].
- [58] J. Fan, M. Reece, and L.-T. Wang, *Non-relativistic effective theory of dark matter direct detection*, *JCAP* **11** (2010) 042, [[arXiv:1008.1591](#)].
- [59] J. Goodman, M. Ibe, A. Rajaraman, W. Shepherd, T. M. P. Tait, and H.-B. Yu, *Constraints on Dark Matter from Colliders*, *Phys. Rev. D* **82** (2010) 116010, [[arXiv:1008.1783](#)].
- [60] M. Beltran, D. Hooper, E. W. Kolb, Z. A. C. Krusberg, and T. M. P. Tait, *Maverick dark matter at colliders*, *JHEP* **09** (2010) 037, [[arXiv:1002.4137](#)].
- [61] A. L. Fitzpatrick, W. Haxton, E. Katz, N. Lubbers, and Y. Xu, *The Effective Field Theory of Dark Matter Direct Detection*, *JCAP* **02** (2013) 004, [[arXiv:1203.3542](#)].
- [62] S. Bhattacharya and J. Wudka, *Effective theories with dark matter applications*, *Int. J. Mod. Phys. D* **30** (2021), no. 13 2130004, [[arXiv:2104.01788](#)].
- [63] D. Borah, N. Das, S. Jahedi, and B. Thacker, *Collider and CMB complementarity of leptophilic dark matter with light Dirac neutrinos*, [[arXiv:2408.14548](#)].
- [64] A. G. Beda, V. B. Brudanin, V. G. Egorov, D. V. Medvedev, V. S. Pogosov, M. V. Shirchenko, and A. S. Starostin, *The results of search for the neutrino magnetic moment in GEMMA experiment*, *Adv. High Energy Phys.* **2012** (2012) 350150.
- [65] **XENON** Collaboration, E. Aprile *et al.*, *Search for New Physics in Electronic Recoil Data from XENONnT*, *Phys. Rev. Lett.* **129** (2022), no. 16 161805, [[arXiv:2207.11330](#)].
- [66] **Borexino** Collaboration, M. Agostini *et al.*, *Limiting neutrino magnetic moments with Borexino Phase-II solar neutrino data*, *Phys. Rev. D* **96** (2017), no. 9 091103, [[arXiv:1707.09355](#)].
- [67] F. Capozzi and G. Raffelt, *Axion and neutrino bounds improved with new calibrations of the tip of the red-giant branch using geometric distance determinations*, *Phys. Rev. D* **102** (2020), no. 8 083007, [[arXiv:2007.03694](#)].

- [68] DESI Collaboration, A. G. Adame *et al.*, *DESI 2024 VI: Cosmological Constraints from the Measurements of Baryon Acoustic Oscillations*, [arXiv:2404.03002](#).
- [69] R. H. Cyburt, B. D. Fields, K. A. Olive, and T.-H. Yeh, *Big Bang Nucleosynthesis: 2015*, *Rev. Mod. Phys.* **88** (2016) 015004, [[arXiv:1505.01076](#)].
- [70] G. Mangano, G. Miele, S. Pastor, T. Pinto, O. Pisanti, and P. D. Serpico, *Relic neutrino decoupling including flavor oscillations*, *Nucl. Phys. B* **729** (2005) 221–234, [[hep-ph/0506164](#)].
- [71] E. Grohs, G. M. Fuller, C. T. Kishimoto, M. W. Paris, and A. Vlasenko, *Neutrino energy transport in weak decoupling and big bang nucleosynthesis*, *Phys. Rev. D* **93** (2016), no. 8 083522, [[arXiv:1512.02205](#)].
- [72] P. F. de Salas and S. Pastor, *Relic neutrino decoupling with flavour oscillations revisited*, *JCAP* **07** (2016) 051, [[arXiv:1606.06986](#)].
- [73] K. Abazajian *et al.*, *CMB-S4 Science Case, Reference Design, and Project Plan*, [arXiv:1907.04473](#).
- [74] CMB-HD Collaboration, S. Aiola *et al.*, *Snowmass2021 CMB-HD White Paper*, [arXiv:2203.05728](#).
- [75] K. N. Abazajian and J. Heeck, *Observing Dirac neutrinos in the cosmic microwave background*, *Phys. Rev. D* **100** (2019) 075027, [[arXiv:1908.03286](#)].
- [76] P. Fileviez Pérez, C. Murgui, and A. D. Plascencia, *Neutrino-Dark Matter Connections in Gauge Theories*, *Phys. Rev. D* **100** (2019), no. 3 035041, [[arXiv:1905.06344](#)].
- [77] C. Han, M. L. López-Ibáñez, B. Peng, and J. M. Yang, *Dirac dark matter in  $U(1)_{B-L}$  with the Stueckelberg mechanism*, *Nucl. Phys. B* **959** (2020) 115154, [[arXiv:2001.04078](#)].
- [78] X. Luo, W. Rodejohann, and X.-J. Xu, *Dirac neutrinos and  $N_{\text{eff}}$* , *JCAP* **06** (2020) 058, [[arXiv:2005.01629](#)].
- [79] D. Borah, A. Dasgupta, C. Majumdar, and D. Nanda, *Observing left-right symmetry in the cosmic microwave background*, *Phys. Rev. D* **102** (2020), no. 3 035025, [[arXiv:2005.02343](#)].
- [80] P. Adshead, Y. Cui, A. J. Long, and M. Shamma, *Unraveling the Dirac neutrino with cosmological and terrestrial detectors*, *Phys. Lett. B* **823** (2021) 136736, [[arXiv:2009.07852](#)].
- [81] X. Luo, W. Rodejohann, and X.-J. Xu, *Dirac neutrinos and  $N_{\text{eff}}$ . Part II. The freeze-in case*, *JCAP* **03** (2021) 082, [[arXiv:2011.13059](#)].
- [82] D. Mahanta and D. Borah, *Low scale Dirac leptogenesis and dark matter with observable  $\Delta N_{\text{eff}}$* , *Eur. Phys. J. C* **82** (2022), no. 5 495, [[arXiv:2101.02092](#)].
- [83] Y. Du and J.-H. Yu, *Neutrino non-standard interactions meet precision measurements of  $N_{\text{eff}}$* , *JHEP* **05** (2021) 058, [[arXiv:2101.10475](#)].
- [84] D. Borah, S. Mahapatra, D. Nanda, and N. Sahu, *Type II Dirac seesaw with observable  $\Delta N_{\text{eff}}$  in the light of  $W$ -mass anomaly*, *Phys. Lett. B* **833** (2022) 137297, [[arXiv:2204.08266](#)].
- [85] D. Borah, S. Jyoti Das, and N. Okada, *Affleck-Dine co genesis of baryon and dark matter*, *JHEP* **05** (2023) 004, [[arXiv:2212.04516](#)].
- [86] S.-P. Li, X.-Q. Li, X.-S. Yan, and Y.-D. Yang, *Cosmological imprints of Dirac neutrinos in a keV-vacuum 2HDM\**, *Chin. Phys. C* **47** (2023), no. 4 043109, [[arXiv:2202.10250](#)].
- [87] A. Biswas, D. K. Ghosh, and D. Nanda, *Concealing Dirac neutrinos from cosmic microwave background*, *JCAP* **10** (2022) 006, [[arXiv:2206.13710](#)].
- [88] P. Adshead, P. Ralegankar, and J. Shelton, *Dark radiation constraints on portal interactions with hidden sectors*, *JCAP* **09** (2022) 056, [[arXiv:2206.13530](#)].

- [89] D. Borah, S. Mahapatra, D. Nanda, S. K. Sahoo, and N. Sahu, *Singlet-doublet fermion Dark Matter with Dirac neutrino mass,  $(g - 2)_\mu$  and  $\Delta N_{eff}$* , *JHEP* **05** (2024) 096, [[arXiv:2310.03721](#)].
- [90] D. Borah, P. Das, and D. Nanda, *Observable  $\Delta N_{eff}$  in Dirac scotogenic model*, *Eur. Phys. J. C* **84** (2024), no. 2 140, [[arXiv:2211.13168](#)].
- [91] N. Das, S. Jyoti Das, and D. Borah, *Thermalized dark radiation in the presence of a PBH:  $\Delta N_{eff}$  and gravitational waves complementarity*, *Phys. Rev. D* **108** (2023), no. 9 095052, [[arXiv:2306.00067](#)].
- [92] H. Esseili and G. D. Kribs, *Cosmological implications of gauged  $U(1)_{B-L}$  on  $\Delta N_{eff}$  in the CMB and BBN*, *JCAP* **05** (2024) 110, [[arXiv:2308.07955](#)].
- [93] L. Angel, P. Escalona, V. Oliveira, C. A. d. S. Pires, and F. S. Queiroz, *Type-II Seesaw Mechanism for Dirac Neutrinos and its Implications on  $N_{eff}$  and Lepton Flavor Violation*, [[arXiv:2502.01760](#)].
- [94] A. Biswas, E. J. Chun, S. Mandal, and D. Nanda, *Phenomenology of Dirac neutrino EFTs up to dimension six*, [[arXiv:2411.17414](#)].
- [95] I. J. Allali, A. Notari, and F. Rompineve, *Dark Radiation with Baryon Acoustic Oscillations from DESI 2024 and the  $H_0$  tension*, [[arXiv:2404.15220](#)].
- [96] **SPT-3G** Collaboration, J. S. Avva *et al.*, *Particle Physics with the Cosmic Microwave Background with SPT-3G*, *J. Phys. Conf. Ser.* **1468** (2020), no. 1 012008, [[arXiv:1911.08047](#)].
- [97] S.-P. Li and X.-J. Xu, *Neutrino magnetic moments meet precision  $N_{eff}$  measurements*, *JHEP* **02** (2023) 085, [[arXiv:2211.04669](#)].
- [98] P. Gondolo and G. Gelmini, *Cosmic abundances of stable particles: Improved analysis*, *Nucl. Phys. B* **360** (1991) 145–179.
- [99] T. Cohen, J. Doss, and X. Lu, *Unitarity bounds on effective field theories at the LHC*, *JHEP* **04** (2022) 155, [[arXiv:2111.09895](#)].
- [100] J. Billard *et al.*, *Direct detection of dark matter—APPEC committee report\**, *Rept. Prog. Phys.* **85** (2022), no. 5 056201, [[arXiv:2104.07634](#)].
- [101] T. R. Slatyer, *Indirect dark matter signatures in the cosmic dark ages. I. Generalizing the bound on s-wave dark matter annihilation from Planck results*, *Phys. Rev. D* **93** (2016), no. 2 023527, [[arXiv:1506.03811](#)].
- [102] I. John and T. Linden, *Cosmic-Ray Positrons Strongly Constrain Leptophilic Dark Matter*, *JCAP* **12** (2021) 007, [[arXiv:2107.10261](#)].
- [103] J. C. Pati and A. Salam, *Lepton Number as the Fourth Color*, *Phys. Rev. D* **10** (1974) 275–289. [Erratum: *Phys.Rev.D* **11**, 703–703 (1975)].
- [104] R. N. Mohapatra and J. C. Pati, *Left-Right Gauge Symmetry and an Isoconjugate Model of CP Violation*, *Phys. Rev. D* **11** (1975) 566–571.
- [105] R. N. Mohapatra and J. C. Pati, *A Natural Left-Right Symmetry*, *Phys. Rev. D* **11** (1975) 2558.
- [106] G. Senjanovic and R. N. Mohapatra, *Exact Left-Right Symmetry and Spontaneous Violation of Parity*, *Phys. Rev. D* **12** (1975) 1502.
- [107] G. Senjanovic, *Spontaneous Breakdown of Parity in a Class of Gauge Theories*, *Nucl. Phys. B* **153** (1979) 334–364.
- [108] R. N. Mohapatra, F. E. Paige, and D. P. Sidhu, *Symmetry Breaking and Naturalness of Parity Conservation in Weak Neutral Currents in Left-Right Symmetric Gauge Theories*, *Phys. Rev. D* **17** (1978) 2462.

- [109] R. N. Mohapatra and R. E. Marshak, *Local B-L Symmetry of Electroweak Interactions, Majorana Neutrinos and Neutron Oscillations*, *Phys. Rev. Lett.* **44** (1980) 1316–1319. [Erratum: *Phys.Rev.Lett.* 44, 1643 (1980)].
- [110] C. S. Lim and T. Inami, *Lepton Flavor Nonconservation and the Mass Generation Mechanism for Neutrinos*, *Prog. Theor. Phys.* **67** (1982) 1569.
- [111] J. F. Gunion, J. Grifols, A. Mendez, B. Kayser, and F. I. Olness, *Higgs Bosons in Left-Right Symmetric Models*, *Phys. Rev. D* **40** (1989) 1546.
- [112] N. G. Deshpande, J. F. Gunion, B. Kayser, and F. I. Olness, *Left-right symmetric electroweak models with triplet Higgs*, *Phys. Rev. D* **44** (1991) 837–858.
- [113] P. Fileviez Perez, *Type III Seesaw and Left-Right Symmetry*, *JHEP* **03** (2009) 142, [[arXiv:0809.1202](#)].
- [114] V. Bernard, S. Descotes-Genon, and L. Vale Silva, *Constraining the gauge and scalar sectors of the doublet left-right symmetric model*, *JHEP* **09** (2020) 088, [[arXiv:2001.00886](#)].
- [115] **ATLAS** Collaboration, G. Aad *et al.*, *Search for a heavy charged boson in events with a charged lepton and missing transverse momentum from pp collisions at  $\sqrt{s} = 13$  TeV with the ATLAS detector*, *Phys. Rev. D* **100** (2019), no. 5 052013, [[arXiv:1906.05609](#)].
- [116] A. Davidson, *B – L as the fourth color within an  $SU(2)_L \times U(1)_R \times U(1)$  model*, *Phys. Rev. D* **20** (1979) 776.
- [117] R. E. Marshak and R. N. Mohapatra, *Quark - Lepton Symmetry and B-L as the U(1) Generator of the Electroweak Symmetry Group*, *Phys. Lett. B* **91** (1980) 222–224.
- [118] A. Masiero, J. F. Nieves, and T. Yanagida, *B – l Violating Proton Decay and Late Cosmological Baryon Production*, *Phys. Lett. B* **116** (1982) 11–15.
- [119] R. N. Mohapatra and G. Senjanovic, *Spontaneous Breaking of Global B – l Symmetry and Matter - Antimatter Oscillations in Grand Unified Theories*, *Phys. Rev. D* **27** (1983) 254.
- [120] W. Buchmuller, C. Greub, and P. Minkowski, *Neutrino masses, neutral vector bosons and the scale of B-L breaking*, *Phys. Lett. B* **267** (1991) 395–399.
- [121] J. Heeck, *Unbroken B – L symmetry*, *Phys. Lett. B* **739** (2014) 256–262, [[arXiv:1408.6845](#)].
- [122] **CMS** Collaboration, A. M. Sirunyan *et al.*, *Search for resonant and nonresonant new phenomena in high-mass dilepton final states at  $\sqrt{s} = 13$  TeV*, *JHEP* **07** (2021) 208, [[arXiv:2103.02708](#)].
- [123] **ATLAS** Collaboration, G. Aad *et al.*, *Search for high-mass dilepton resonances using 139  $fb^{-1}$  of pp collision data collected at  $\sqrt{s} = 13$  TeV with the ATLAS detector*, *Phys. Lett. B* **796** (2019) 68–87, [[arXiv:1903.06248](#)].
- [124] **LHCb** Collaboration, R. Aaij *et al.*, *Search for  $A' \rightarrow \mu^+ \mu^-$  Decays*, *Phys. Rev. Lett.* **124** (2020), no. 4 041801, [[arXiv:1910.06926](#)].
- [125] **BaBar** Collaboration, J. P. Lees *et al.*, *Search for a Dark Photon in  $e^+e^-$  Collisions at BaBar*, *Phys. Rev. Lett.* **113** (2014), no. 20 201801, [[arXiv:1406.2980](#)].
- [126] M. Cadeddu, N. Cargioli, F. Dordei, C. Giunti, Y. F. Li, E. Picciau, and Y. Y. Zhang, *Constraints on light vector mediators through coherent elastic neutrino nucleus scattering data from COHERENT*, *JHEP* **01** (2021) 116, [[arXiv:2008.05022](#)].
- [127] P. Coloma, P. Coloma, M. C. Gonzalez-Garcia, M. C. Gonzalez-Garcia, M. Maltoni, M. Maltoni, J. a. P. Pinheiro, J. a. P. Pinheiro, S. Urrea, and S. Urrea, *Constraining new physics with Borexino Phase-II spectral data*, *JHEP* **07** (2022) 138, [[arXiv:2204.03011](#)]. [Erratum: *JHEP* 11, 138 (2022)].
- [128] J. Blumlein and J. Brunner, *New Exclusion Limits for Dark Gauge Forces from Beam-Dump Data*, *Phys. Lett. B* **701** (2011) 155–159, [[arXiv:1104.2747](#)].

- [129] J. D. Bjorken, S. Ecklund, W. R. Nelson, A. Abashian, C. Church, B. Lu, L. W. Mo, T. A. Nunamaker, and P. Rassmann, *Search for Neutral Metastable Penetrating Particles Produced in the SLAC Beam Dump*, *Phys. Rev. D* **38** (1988) 3375.
- [130] J. D. Bjorken, R. Essig, P. Schuster, and N. Toro, *New Fixed-Target Experiments to Search for Dark Gauge Forces*, *Phys. Rev. D* **80** (2009) 075018, [[arXiv:0906.0580](https://arxiv.org/abs/0906.0580)].